Balanced and Unbalanced Circulations in a Primitive Equation Simulation of a Midlatitude MCC. Part I: The Numerical Simulation

PETER Q. OLSSON AND WILLIAM R. COTTON

Department of Atmospheric Science, Colorado State University, Fort Collins, Colorado

(Manuscript received 7 August 1995, in final form 27 June 1996)

ABSTRACT

A midlatitude mesoscale convective complex (MCC), which occurred over the central United States on 23–24 June 1985, was simulated using the Regional Atmospheric Modeling System (RAMS). The multiply nested-grid simulation agreed reasonably well with surface, upper-air, and satellite observations and ground-based radar plots. The simulated MCC had a typical structure consisting of a leading line of vigorous convection and a trailing region of less intense stratiform rainfall. Several other characteristic MCC circulations were also simulated: a divergent cold pool in the lower troposphere, midlevel convergence coupled with a relatively cool descending rear-inflow jet, and relatively warm updraft structure, and a cold divergent anticyclone in the tropopause region. Early in the MCC simulation, a mesoscale convectively induced vortex (MCV) formed on the eastern edge of the convective line. While frequently associated with MCCs and other mesoscale convective systems (MCSs), MCVs are more typically reported in the mature and decaying stages of the life cycle. Several hours later, a second MCV formed near the opposite end of the convective line, and by the mature phase of the MCC, these MCVs were embedded within a more complex system-wide vortical flow in the lower troposphere.

Analysis of the first MCV during its incipient phase indicates that the vortex initially formed near the surface by convergence/stretching of the large low-level ambient vertical vorticity in this region. Vertical advection appeared largely responsible for the upward extension of this MCV to about 3.5 km above the surface, with tilting of horizontal vorticity playing a secondary role. This mechanism of MCV formation is in contrast to recent idealized high-resolution squall line simulations, where MCVs were found to result from the tilting into the vertical of storm-induced horizontal vorticity formed near the top of the cold pool.

Another interesting aspect of the simulation was the development of a banded vorticity structure at midtropospheric levels. These bands were found to be due to the apparent vertical transport of zonal momentum by the descending rear-to-front circulation, or rear-inflow jet. An equivalent alternative viewpoint of this process, deformation of horizontal vorticity filaments by the convective updrafts and rear-inflow jet, is discussed.

Part II of this work presents a complementary approach to the analysis presented here, demonstrating that the circulations seen in this MCC simulation are, to a large degree, contained within the nonlinear balance approximation, the related balanced omega equation, and the PV as analyzed from the PE model results.

1. Introduction

Since Maddox (1980) first posited the mesoscale convective complex (MCC), considerable research has been focused on both observational studies and numerical simulations of MCCs and other smaller, yet dynamically similar mesoscale convective systems (MCSs). MCCs and MCSs exhibit a broad commonality of structure (Houze et al. 1990) with several ubiquitous circulations (Bartels and Maddox 1991; Rutledge 1991).

One of the more striking features present in several MCS case studies is the existence of a mesoscale convective vortex (MCV) (e.g., Leary and Rappaport 1987; Zhang and Fritsch 1988; Menard and Fritsch 1989; Brandes 1990; Johnson and Bartels 1992; Fritsch et al. 1994), usually observed in the mature-to-decaying MCC or MCS. Bartels and Maddox (1991) observed that the parent storms of MCVs found in their studies, while all having quasi-circular cloud shields, showed significant diversity in longevity, size, and cloud-top thermal structure. An MCV generated within an MCC has been suggested (Fritsch et al. 1994) as a mechanism to enhance tropical cyclogenesis. The MCV has a warm core structure similar to that of a tropical cyclone and provides an enhanced inertial stability that makes the diabatic heating more efficient at producing balanced, rotational flow. Recently Davis and Weisman (1994) and Skamarock et al. (1994, hereafter SWK) have performed three-dimensional convection-resolving primitive equation (PE) simulations of idealized MCV-producing squall lines. These studies found that MCVs could be produced in horizontally homogeneous domains with high CAPE and weak, shallow shear.

The circulations and thermal structure that typify the

Corresponding author address: Dr. Peter Q. Olsson, Geophysical Institute, University of Alaska Fairbanks, P.O. Box 757320, Fairbanks, AK 99775-7320.
E-mail: peter.olsson@gi.alaska.edu

MCC hint that such disturbances might reasonably obey, at least in the more organized mature and dissipating stages, a particular subset of the primitive equations of motion. Recent work (e.g., Raymond 1992; Davis and Weisman 1994; Jiang and Raymond 1995) has suggested that these systems are to a large degree balanced; that is, the mesoscale circulations and thermal structure comprising the MCC mutually evolve in near agreement with a balance condition. Davis and Weisman (1994) evaluated idealized squall line simulations within the context of balanced dynamics. Chen and Frank (1993) performed numerical simulations of MCCs using an idealized ''typical'' environment and analyzed the evolution of vortical flow features.

While idealization of the MCC genesis environment proves a valuable aid in interpretation of the results, the inherent simplifications and presuppositions may bias the outcome in subtle yet important ways. As an extension of this previous work, and to address these possible shortcomings, the approach used here was to simulate an MCC in the observed, fully variable three-dimensional environment, making such modifications only as were required to render the subsequent balanced analysis tractable and the numerical computations feasible. The intent of this and a companion paper (Olsson and Cotton 1997; hereafter referred to as Part II) is to present results of a numerical simulation of an observed MCC, consider the processes leading to the formation of MCVs and midlevel vorticity banding in the simulated MCC and consider the results in the context of balanced dynamics.

2. Model structure and experiment design

a. Model description

The simulation of the 23–24 June 1985 MCC was performed using RAMS (Regional Atmospheric Modeling System), a nonhydrostatic PE model. The salient features of the model as it is applied to this particular study will be discussed here. For a more thorough description of the model see Pielke et al. (1992).

The fields used to initialize the simulation were obtained by compositing several different datasets. The large-scale background features were obtained from European Center for Medium-Range Forecasting (ECMWF) gridded analyses. To resolve finer-scale features, rawinsonde and surface observation datasets were also analyzed. The RAMS ISAN (ISentropic ANalysis) package (Pielke et. al. 1992), which utilizes Barnes (1973) objective analysis on isentropic surfaces, was used to assimilate the upper-air and surface meteorological data. This composite initialization was then interpolated onto the RAMS (x,y,σ_z model grid, where all fields are adjusted to hydrostatic balance. No attempt was made to introduce any further balance in the initial fields.

Intermediate datasets at 12-h intervals, created by the same method used to produce the initial fields, provided the time-dependent boundary conditions. Using a Newtonian relaxation technique (Davies 1983), tendency terms were computed and applied to points on and near the upper boundaries of all grids and the lateral boundaries of grid 1, ''nudging'' them to the observed values.

The Tremback and Kessler (1985) soil model was used in this simulation, with 11 vertical levels located from -1 cm to -1 m. This model predicted both surface heat and surface moisture fluxes, and worked in concert with the Chen and Cotton (1983) radiation model, which updated radiative fluxes throughout the model domain every 900 s.

Some data concerning vegetation type and coverage and soil moisture in the area of interest were available for this time period. A vegetation-type dataset obtained from NCAR contained spatial distributions of 11 primary vegetation types at a 5-min lat./long. resolution. These data were interpolated onto the model grids and then converted to the vegetation classification used in the model (RAMS uses 18 vegetation types). Within this classification, various quantities such as leaf-area index and shaded soil fraction are diagnosed.

Soil moisture information was obtained from the USDA publication, Weekly Crop Bulletin, which contains weekly maps of soil moisture index for the continental United States. The soil moisture index data were manually transferred to a lat./long. gridded dataset at 1° resolution. This dataset was then filtered and interpolated onto the model grid where it was converted, using a simple linear transformation, into a soil moisture percentage. The result produced credible soil moisture variations and gradients, which were in good qualitative agreement with the soil moisture index values.

As the horizontal scale of convective motions is on the order of a kilometer, a good deal smaller than the finest horizontal grid spacing used here, a convective parameterization was required. The level 2.5*w* convective adjustment scheme (Weissbluth and Cotton 1993) was employed for this simulation. A summary of this scheme appears in the appendix.

b. Model configuration

RAMS uses a terrain-following vertical coordinate system. All three grids contained 32 vertical levels with a stretched vertical grid spacing (no nesting was done in the vertical). For a grid column where terrain height was zero the lowest two model levels had a separation of 175 m, each succeeding grid spacing being a factor of 1.1 times larger, until a maximum grid spacing of 1000 m was reached. From that level to the model top near 20.5 km, the vertical grid spacing was kept constant at 1000 m.

The 24-h simulation period started at 1200 UTC 23 June 1985 (designated 23/1200 here for simplicity), and terminated at 1200 UTC 24 June (24/1200). Use was made of the two-way interactive multiple nested-grid

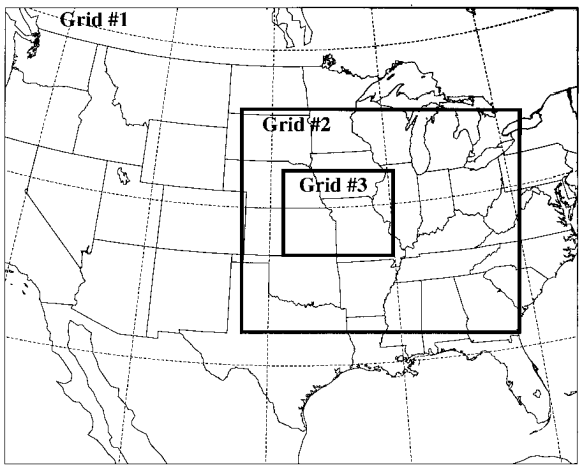

FIG. 1. Relative locations of the model grids. The interior xpoints of grid 2 constitute the horizontal domain on which the balance diagnostics are performed.

capability of RAMS (Walko et al. 1995). The simulation was initialized with two grids and at 23/1800, a third grid was added in the region of the system to better simulate the storm-scale flow features. Figure 1 shows the relative geographic locations of the grids, and Table 1 contains a summary of the various grid properties.

c. Experiment design

Since one of the goals of this simulation is to provide a dataset amenable to analysis in the context of balanced dynamics (as described in Part II) the experiment design incorporates some special features. In terms of the balanced dynamics diagnosis and associated potential vorticity (PV) invertibility problem, probably the most stringent requirement is the need for quasi-balanced conditions at the lateral boundaries throughout the simulation.[1] For this reason, the convective parameterization was active only on grid 3, while the inversion was performed on grid 2. The grid structure was designed such that all grid 2 boundaries were separated from the simulated MCC by a distance of at least Rossby radius λ_R, this length being an *e*-folding scale or ''radius of action'' for boundary effects (Hoskins et al. 1985). The desired result is that the strong perturbations induced by the simulated MCC are generally contained well within the grid 2 interior.

A consequence of restricting convection to grid 3 is that observed convection occurring outside the region spanned by grid 3 was not reproduced in the simulation. Most significantly, this means that the more western MCS of 23–24 June (description follows in section 3) was not simulated. Since this system occurred near the western boundary of grid 2, its unbalanced flow would certainly have seriously perturbed the wind and thermal structure near the grid 2 boundaries. In addition to that MCS in Kansas and Oklahoma, scattered convection occurred in the late afternoon in southern Illinois, eastern Colorado, Texas, and elsewhere. This convection was generally transient and by about 24/0200 infrared satellite images (Stensrud and Maddox 1988, hereafter SM) show that the two mesoscale systems were the only significant convection in the central United States.

Some temporal constraints were also placed on the simulated convection. This was done for two reasons. First, the RAMS initial wind fields do not necessarily satisfy mass continuity; that is, the initial horizontal divergence field is incompatible with the initial vertical motion field ($w = 0$ everywhere). This results in spurious vertical motion fields as the model achieves continuity. The second reason again relates to the PV inversion. Convection had been occurring along the front in Iowa and Illinois (the focus for the MCC later in the day) from the early morning on. In sensitivity studies, capturing this morning convection confused the interpretation of the balanced flow during the upscale growth of the MCC. For these reasons the convective parameterization was not activated until 7 h of simulation time. In an attempt to reproduce some of the low-level effects of this earlier convection, the soil moisture was enhanced in central and eastern Iowa and western Illinois, and the soil temperature was decreased in the top two model levels by 5°C, consistent with typical perturbations observed in the surface model as the result of moderate precipitation. These modifications were done to grid 3 when it was spawned, and were fed back onto the coarser grids via the grid interaction. No modifications were made to the atmospheric fields.

[1] As will be discussed in Part II, the model winds and geopotential at these boundaries are used to formulate boundary conditions for the PV inversion. The global nature of the solution results in the boundary conditions having an effect on the solution well into the interior of the domain.

TABLE 1. A summary of the RAMS model configuration.

	Grid 1	Grid 2	Grid 3
Grid spacing (Δx)	75 km	25 km	8.33 km
Grid dimensions ($x \times y$) km	4050 × 3225	1975 × 1600	833.3 × 633.3
Number of points ($x \times y$)	55 × 44	80 × 65	101 × 77
Vertical levels	32	32	32
Time step (Δt)	90 s	45 s	22.5 s
Convective parameterization	none	none	level 2.5 *w*

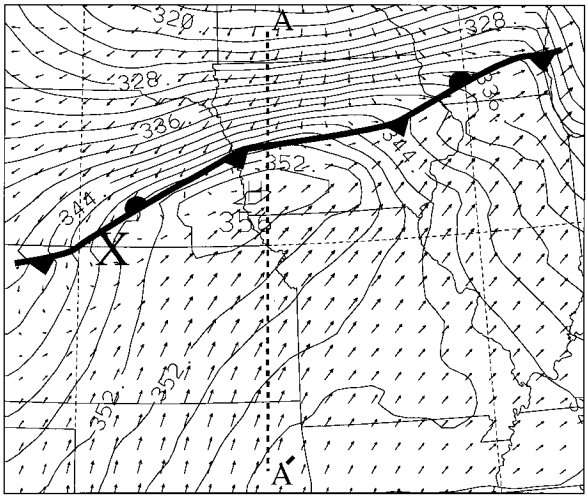

FIG. 2. Wind vectors and contours of equivalent potential temperature at the surface at 23/1900. The contour level for θ_e is 2K, and the maximum wind vector in the figure corresponds to 10 m s^{-1}. The bold **X** indicates the location of the surface low pressure center. (In this and subsequent figures that display vectors, the vectors appear at every other grid point in both dimensions.)

3. Storm description

The dominant synoptic features over the southern Great Plains on 23 June 1985 were a weak 500-mb ridge, a stationary surface front extending from southern Illinois through central Iowa and westward into Nebraska, and a persistent, strong low-level jet (LLJ) at 850 mb, transporting moisture from the Gulf of Mexico well into the central United States (see SM, Figs. 1 and 2). The winds were light at 500 mb over the southern Great Plains, but increased significantly with height, giving a large vertical shear in the upper troposphere. A significant horizontal N–S velocity gradient also existed, with 500-mb winds increasing from less than 5 m s^{-1} over southern Missouri to almost 25 m s^{-1} over central Minnesota, resulting in a weakly inertially stable to slightly unstable environment over the MCC genesis area.

The convective outbreak that occurred over the central Great Plains on 23–24 June was comprised of two mesoscale systems. During the daylight hours of 23 June, the frontal boundary was the focus for convection from eastern Nebraska eastward to Illinois and Indiana. The larger of the two systems, and the focus of the modeling study, was an MCC that originated at around 23/2030 as a line of convection extending along the front from south-central Iowa to eastern Nebraska. Tornadoes and local flooding occurred south of Des Moines in the late afternoon with precipitation rates over 100 mm h^{-1}, while about 200 km westward along the front numerous tornadoes and three lightning-related fatalities were reported near the Iowa–Nebraska border. As the MCC slowly propagated south and east during its 9 h lifetime, the system lost much of its initial linear organization. By 24/0900, precipitation from the system had largely ceased, though the remnant cloud shield was still evident in IR satellite imagery for several hours.

The smaller and more western of the two systems initiated in west-central Kansas and propagated SSE directly over the PRE-STORM[2] surface observation network in south-central Kansas and Oklahoma. It is interesting to note that MCVs were observed in both the small, western MCS (Johnson and Bartels 1992) and the larger MCC (Meitín and Cunning 1985), even though the mesoscale environments were considerably different.

4. The 23–24 June MCC simulation: Genesis stage

By late morning, even prior to the spawning of grid 3, the model had produced significant stratus cloud along the cold front in central Iowa as a result of the strong low-level convergence occurring there. The convective parameterization was activated at 23/1900. Figure 2 shows the predicted surface equivalent potential temperature (θ_e) field and horizontal winds at this time, along with the cold front and surface low pressure center. The tongue of high-valued θ_e air is quite apparent in this figure, with values of $\theta_e \geq 350$ K. The LLJ, which maintains and reinforces the high θ_e values, is largely contained within the boundary layer θ_e ridge. The location of the surface low pressure center along the Nebraska–Kansas border agrees fairly well with the 23/2100 mesoscale analysis of Johnson et al. (1989, see their Fig. 1) but is somewhat south of the location in the NWS 23/1800 surface analysis. The simulated circulation around the low is not as closed and cyclonic as was observed.

Figure 3 shows the simulated thermodynamic profile for a model point near Beatrice, Nebraska, (BEA) at 23/2000, prior to the triggering of convection at that grid point. This sounding is fairly representative of the thermodynamic environment south of the cold front. The simulated surface and dewpoint temperatures near BEA were 35°C and 20°C, which agree well with the observed values of 36°C/21°C at this time.

By 23/2000, an area of convection had developed in east-central Iowa along the simulated cold front. (Though contemporaneous observations indicate that precipitation was not occurring here, late morning surface reports from this region recorded heavy rain, damaging winds, and golf ball–sized hail). The strong response of the convective parameterization was due to the combination of large resolved vertical velocities ($>$ 8 cm s^{-1}) and high CAPE values. As this broken convective line drifted eastward over the moist soil in eastern Iowa, where sensible surface heat fluxes were weak-

[2] PRE-STORM (Preliminary Regional Experiment for Stormscale Operational Research Meteorology) was a multiagency field program conducted in May and June 1985 in Oklahoma and Kansas to study convective storms on the mesoscale (Meitín and Cunning 1985).

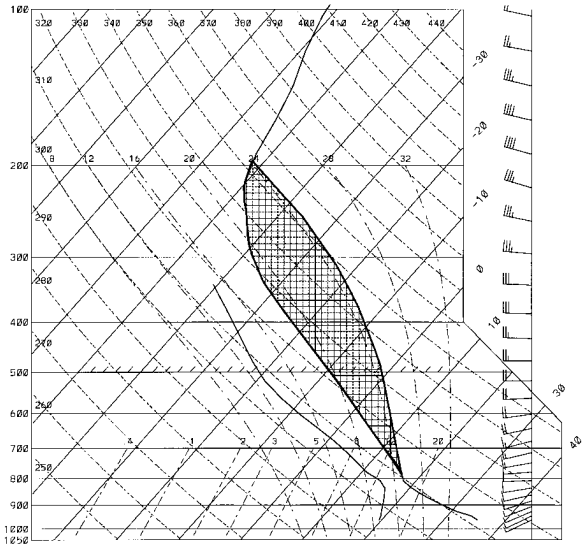

FIG. 3. The skew-*T* thermodynamic diagram for the simulated sounding near Beatrice, NE, at 23/2100. The hatched region represents the positive area of buoyant energy. The CAPE exceeds 2700 J kg^{-1}.

er and ambient CAPE values smaller, the parameterized convection subsided.

Soon after this time, the convection directly associated with the subsequent MCC developed in two distinct regions along the cold front. Shortly after 23/2000 an E–W convective line developed along the eastern half of the Iowa–Missouri border, just to the south of the cold front, continuing WSW about 100 km into SE Nebraska. The initial location of this new convection coincided with the θ_e maximum in Fig. 2.[3] Another shorter line, with a N–S orientation, was developing in central Iowa over and to the north of the front.

Between 23/2030 and 23/2200, both lines continued to intensify. The plots in Fig. 4 show midtropospheric horizontal cross sections of relative vorticity, vertical velocity, and PV at 23/2100. In Fig. 4b, the vertical velocity field clearly shows the orientation of the two convective lines. Both the N–S line and strengthening E–W line are in evidence, as are the areas of compensating mesoscale subsidence, indicated by the dashed (negative) contours.

The relative vorticity associated with the E–W line at 23/2100 shows the presence of large, positive relative vorticity, more or less collocated with the large convective updrafts, and a narrow trailing band of very negative relative vorticity. Note that the *ambient* relative vorticity field at this level is somewhat negative, due to

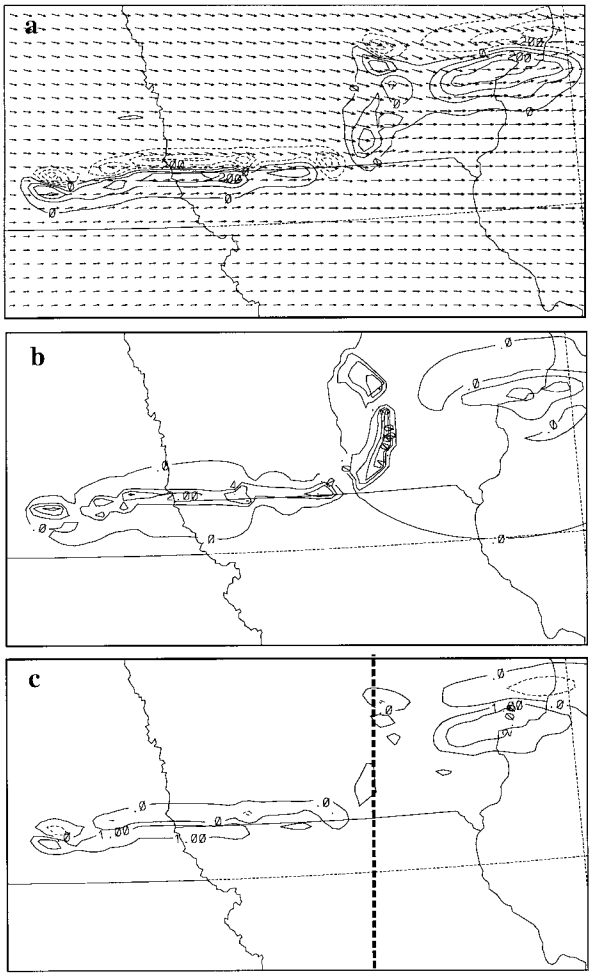

FIG. 4. All plots at time 23/2100 and height of 5220 m ASL. (a) Horizontal winds (max vector 26 m s^{-1}) and relative vorticity, with a contour level of 10^{-4} s^{-1}. (b) Vertical velocity, with a contour level of 1.0 m s^{-1}. (c) PV, with a contour level 1 PVU (1 PVU = 10^{-6} m^2 s^{-1} K kg^{-1}, Hoskins et al. 1985). All plots have the negative coutours dashed.

the zonal wind increasing to the north. Regions within closed dashed contours, where vertical vorticity $\zeta < -1.0\times10^{-4}$ s^{-1}, represent areas that are potentially inertially unstable.

The vorticity maximum along the Iowa/Illinois border in Fig. 4a is a remnant of the first short-lived burst of convection at 23/2000, and is advecting out of Iowa in the brisk westerly flow. This feature, while decoupled from any parameterized convection, had maximum midtropospheric updrafts of almost 2 m s^{-1} and continued to produce light stratiform precipitation as it propagated eastward along the cold-frontal boundary.

Figure 5a (23/2230) shows contours of vertical velocity variance, $\overline{w'w'}$, the variable predicted by the convective parameterization. (Large values of $\overline{w'w'}$ are found in regions where the convective parameterization is currently, or has recently been, active.) Figure 5b

[3] In their climatology of the MCCs of 1985, Augustine and Howard (1988) list the time of ''first storms'' as 2030 UTC. Our review of available satellite images found the time of first storms was indeterminate, as vigorous convection had been occuring in the MCC genesis region almost continuously since dawn.

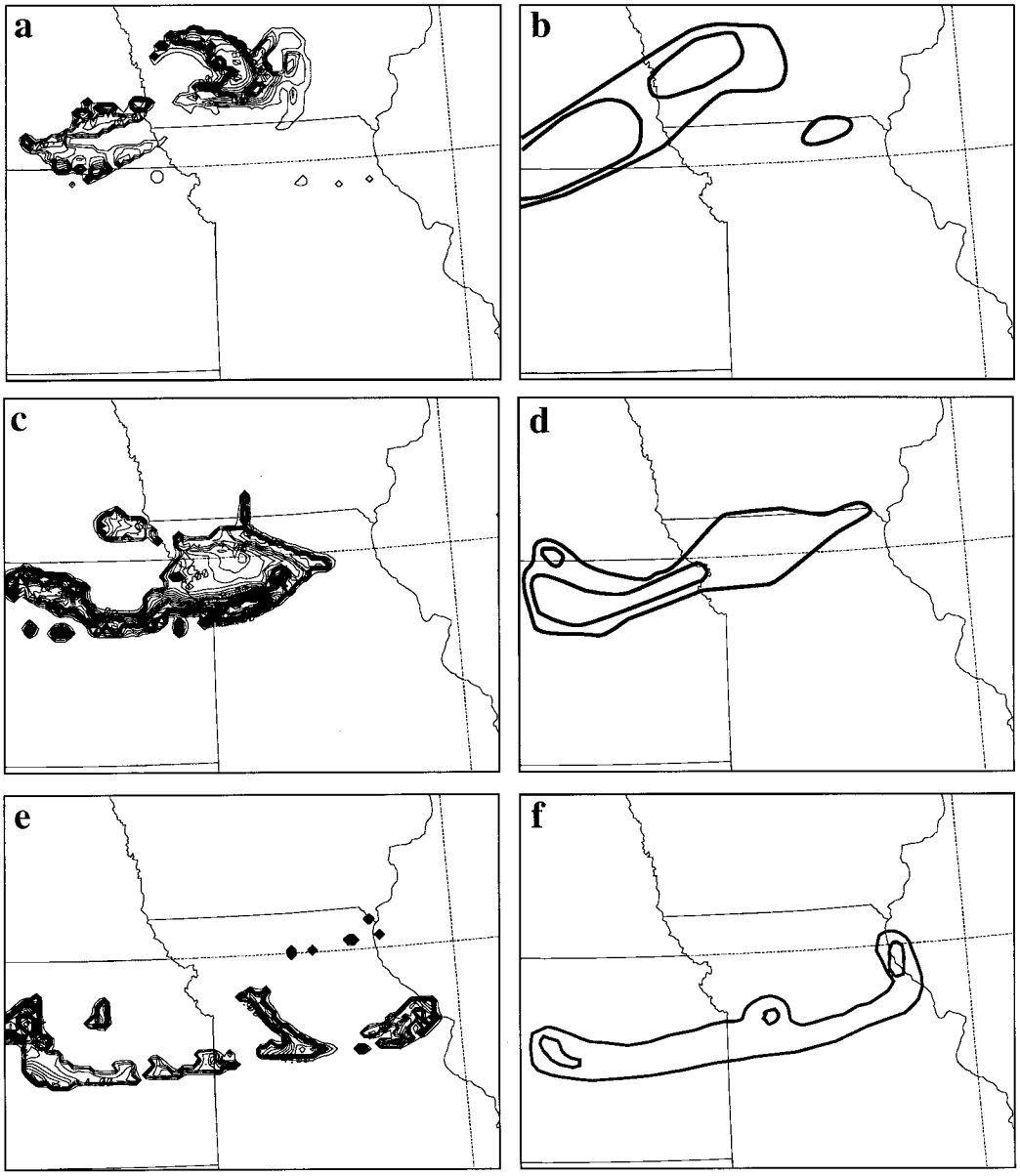

FIG. 5. (a) Surface $\overline{w'w'}$ at 23/2230 with contours are 4 m^2 s^{-2}. (The convective parameterization uses $\overline{w'w'}$ as a trigger function. Hence, locations where $\overline{w'w'}$ is large indicate, in a short-term time-averaged sense, where the parameterized convection is occurring in the model simulation. (b) WSR 57 observed radar echoes, also at 23/2230. Contours are VIP levels 3 and 5, corresponding to 40.5 and 50.5 dbz, respectively (National Weather Service 1982). (c) Same as in (a) except $\overline{w'w'}$ contours at 2 m^2 s^{-2}, time 24/0230. (d) Same as (b) except time 24/0230. (e) and (f) As in (c) and (d) except time 24/0530.

shows the level 3 and level 5 VIP contours at 23/2230, corresponding to 40.5 and 50.5 dBz, respectively (National Weather Service 1982). While the vigorous simulated convection over Iowa is displaced about 50–75 km to the east relative to the observations, comparison of Figs. 5a and 5b show that the overall pattern of parameterized and observed convection agrees reasonably well. Figure 5a shows a new band of convection developing in extreme SE Nebraska, while the original E–W oriented line behind has lost continuity in SW Iowa. Though parameterized convection continued behind the new line for about another hour, it was much less vigorous, since the flow of high θ_e air fueling the initial convection was intercepted by the newly developed line to the south.

The N–S convective line in south-central Iowa broadened considerably and by 23/2230 was of almost the same dimensions latitudinally and longitudinally. The simulated convection occurring in this region at this time was very intense, with rainfall rates exceeding 30

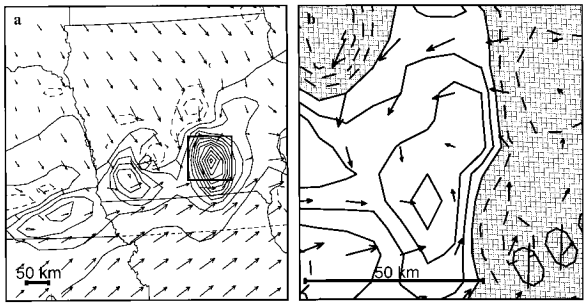

FIG. 6. (a) Simulated relative vorticity and horizontal winds (grid 2) near 1500 m AGL, 23/2230, with the maximum wind speed 28 m s^{-1} and vorticity contour level of 0.5×10^{-4} s^{-1}, dashed lines negative. This level was near the cloud base of the convective cells. (b) Grid 3 vertical velocity and winds at 23/2230 at 270 m AGL, location of plot shown in (a). The maximum wind vector is 22 m s^{-1} and the contour level for vertical velocity is 5 cm s^{-1}, cross-hatched area negative. The vortex in this figure lies almost directly under the vorticity maximum depicted in (a).

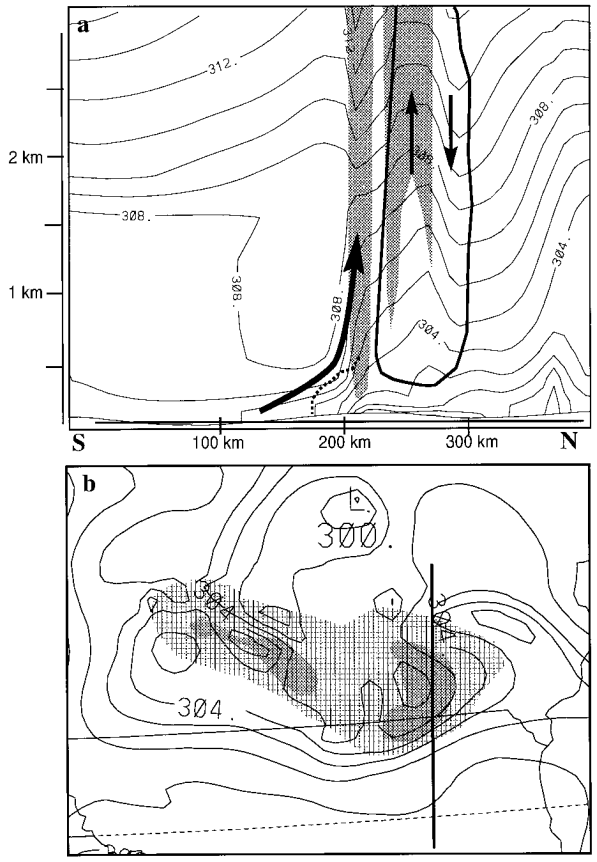

FIG. 7. (a) North–south cross section of θ through the MCV at 24/0000 in the lowest 3 km of the domain. The gray shading indicates updrafts > 0.5 m s^{-1}. The heavy line is the relative vorticity $= 5f$ contour and indicates the position of the MCV. The dashed line indicates the approximate forward location of the cold pool. (b) The θ contours (1°C increments) at 24/0000, 490 m AGL. The cross hatching indicates the region where total condensate mixing ratio values are nonzero, and the solid gray shading indicates values exceeding 2 g kg^{-1}. At this level (below cloud base) total condensate is equivalent to precipitation. The heavy N–S oriented line indicates the location of the cross section in (a).

mm h^{-1}. Observations from this region also indicate very heavy precipitation, with over 120 mm of rainfall occurring in portions of Madison, Clark, and Warren Counties of Iowa in the late afternoon, causing widespread flooding of local streams. Three tornadoes were reported, F0 to F1 on the Fujita (1971) intensity scale, as were numerous funnel clouds and large hail.

The simulation developed a mesovortex in this region, with a closed (system-relative) circulation extending from near the surface to about 4000 m. Figure 6a (23/2230) shows the relative vorticity at about 1500 m AGL, approximately the level of the convective cloud base in this region. The vortex is quite apparent with a relative vorticity maximum greater than 6.5×10^{-4} s^{-1}. In Fig. 6b the vertical velocity at 275 m AGL (23/2230) is shown. (Location of plot in Fig. 6b is denoted by box in Fig. 6a, note difference in scale.) The vortex center in Fig. 6b is located directly beneath the vorticity maximum at 1500 m. The vertical velocity field (not shown) within the closed vortex circulation at 1500 m is almost exclusively positive, with maximum (grid 3) values exceeding 1 m s^{-1}. By contrast, the vertical motion field at 275 m reveals significant downward motion along the eastern edge of the vortex with a vertical velocity maximum ($w = 0.18$ m s^{-1}) near the center of the vortex at this level. The relatively strong downdraft in the NW corner of Fig. 6b is also a region of very depressed θ_e values and represents the beginning stages of a descending rear inflow. This is also in evidence in Fig. 6a to the northwest of vorticity maximum, where strong downward motion is collocated with the negative (dashed) region of vorticity. The updraft strength within the vortex at 1500 m was fairly modest compared to the much larger values at the same level in the squall line to the west. The warm-core vortex (> 3°C at 3000 m) had a more stable vertical thermodynamic profile at low and middle levels, which would act to inhibit the updraft in this region. The early development of this mesovortex will be examined in section 6.

By 24/0000 the mesovortex had become somewhat decoupled from the leading line of the convection. Figure 7a (24/0000) shows a N–S cross section of potential temperature θ through the squall line and MCV[4] in the lowest 3 km of the domain. The MCV is separated from the leading convective updrafts by a strong downdraft region. A similar decoupling was seen in the explicit squall line simulations of SWK. The MCV contains

[4] There is no clear convention as to the distinction between the terms ''mesovortex'' and ''MCV'' as both features may be the result of convection. For lack of a rigorous definition, here the vortex is referred to as an MCV when its horizontal extent exceeds 100 km at some level.

regions of both upward and downward motion at this time and may be characterized as cold-core, in contrast to the warm-core structure 90 min earlier.

Figure 7b shows θ and total condensate r_c (equivalent to precipitation mixing ratio below cloud base) at 490 m AGL. The solid gray shading indicates areas where $r_c > 2$ g kg^{-1}. Note that while the east side of the MCV lies within one of these regions, the vertical velocity in the lower reaches of the MCV is relatively small and in some places even negative. Also, since the MCV is now behind the leading convective line, it is cut off from the high θ_e values associated with LLJ. At this time, the precipitation rate within the MCV region was at its maximum. Observational studies (e.g., Leary and Rappaport 1987; Menard and Fritsch 1989) and other numerical simulations (e.g., Zhang and Fritsch 1988; Zhang et al. 1989) have found relatively large precipitation rates associated with MCVs. The θ fields in Figs. 7a and 7b clearly show a well-developed cold pool at 490 m. While the simulation did produce a cold pool, with model surface temperatures behind the gust front about 4 °C cooler than those south of the system, this cooling was only about half that observed.

The evolution of PV

A cross section of PV in the troposphere and lower stratosphere is shown at 23/2000 in Fig. 8a, just prior to the first convection in the simulation. This cross section is located along the line *AA′* in Fig. 2, and passes through the surface front in western Iowa. The well-mixed, and in some locations superadiabatic, convective boundary layer is apparent in approximately the lowest 1.5 km, the top of this layer being the PV = 0.0 contour. A region of relatively enhanced lower-tropospheric PV (> 0.6 PVU) associated with the horizontal frontal flow field is seen between 200 and 500 km in the horizontal. This is also a region of mesoscale low-level positive vertical motion (Fig. 8b). The ''pre-MCC'' mesoscale environment, that region from -200 km to about 400 km in the horizontal, is characterized, in the region south of the frontal zone, by a weak PV field (PV < 0.3 PVU) up to a height of 8 km. This is consistent with the climatologically favorable MCC environment (Maddox 1983; Velasco and Fritsch 1987; Augustine and Howard 1991) being under the a broad midtropospheric pressure ridge. Here the low PV values are due to *both* the increasing westerly winds toward the north (weak inertial stability) and the pattern of warm advection at the surface (weak static stability). Both features are typical of the MCC environment (Maddox 1983; Velasco and Fritsch 1987; Cotton et al. 1989; Augustine and Howard 1991; Blanchard 1994).

A N–S cross section of PV appears in Fig. 9a at time 23/2100, its relative location indicated by the heavy dashed line in Fig. 4c. This cross section is aligned parallel to, and behind the leading edge of, the N–S line in SE Iowa. The developing MCV is evidenced by the

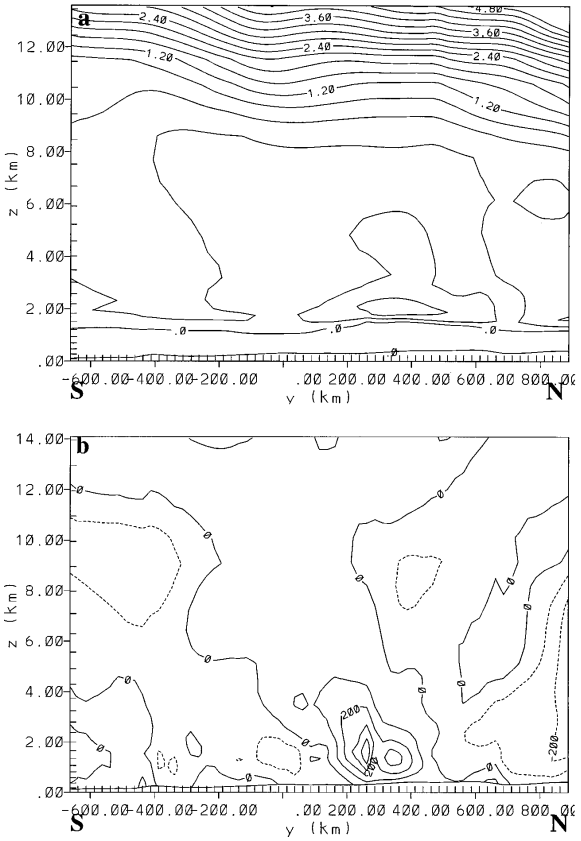

FIG. 8. North–south vertical cross sections of (a) PV and (b) vertical velocity at time 23/2000. The location of the cross section is along the line AA′ in Fig. 2. The PV contour level in (a) is 0.3 PVU and only positive values are contoured. The vertical velocity contour level in (b) is 1 cm s^{-1}, with negative contours dashed and the contour labels are $\times 10^2$. (Note that the top of the model domain extends beyond the top of the figures).

positive PV anomaly with PV > 1 PVU between 2 and 5.5 km in height and 300 to 375 km in the horizontal. A negative upper-tropospheric/lower-stratospheric anomaly with large negative (dashed contour) PV has developed south of the convective line. Inspection of Fig. 10 (near the tropopause), reveals this region of large negative PV is colocated with both the anticyclonic turning of the ambient winds as they were blocked and deflected by the developing high pressure and with the detraining storm outflow. South of the E–W oriented line along the Iowa–Missouri border, the tropopause wind had developed a significant northerly component. Unlike the N–S-oriented line farther to the east with its well-developed upstream stagnation zone, the outflow from the E–W line does not seem to present a significant block to the ambient flow.

5. The mature stage and dissipation

After a brief diminution in convective activity between 24/0000 and 24/0100 the convection again strengthened. In the period from 23/2300 to 24/0230,

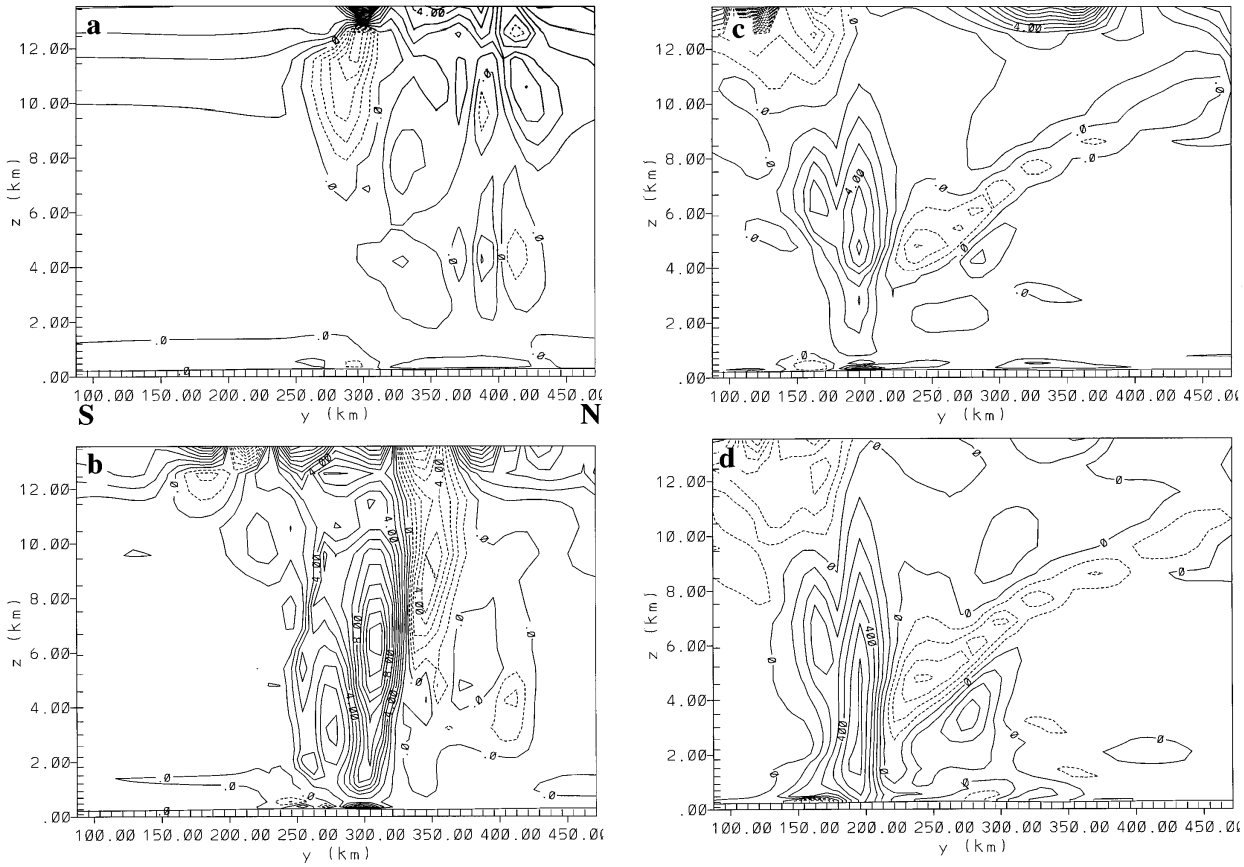

FIG. 9. Panels (a), (b), and (c) show cross sections of PV at times 23/2100, 24/0000, and 24/0230, respectively. The cross sections are located along the dashed line in Fig. 4, with contours at 1 PVU increments. (d) Relative vorticity (contours at 10^{-4} s^{-1}) at 24/0230.

the squall line continued to propagate south and east, with the western end in Kansas/Nebraska propagating southward more rapidly. During this time, the overall organization of the system became altered from the two distinct lines noted before to a more continuous structure with a line of strong convection along the leading edge. Figure 11 and 12 contain midtropospheric cross sections of the MCC at 24/0000 and 24/0230, respectively. The vertical velocity at 24/0000 (Fig. 11b) shows indications of this transition, with three large vertical velocity maxima; a crescent-shaped maximum in SE Iowa associated with the MCV; a second in south-central Iowa; and a third, smaller, elongated w maximum associated with the convection along the far eastern common border of Nebraska and Kansas. By 24/0230, 2.5 h later, the vertical velocity (Fig. 12b) shows a more linear maximum along the leading edge of the convection and a much larger region of weaker mesoscale ascent.

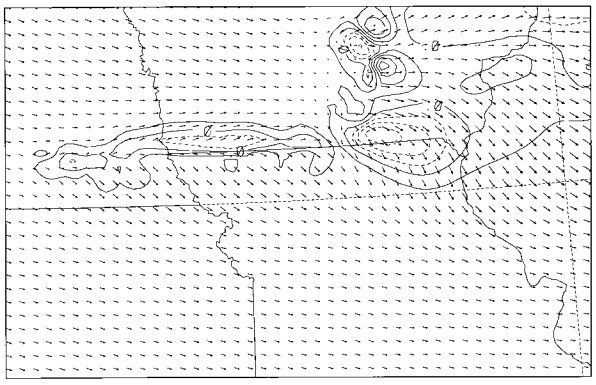

FIG. 10. Winds and PV (23/2100, 1 PVU increments) at 10.5 km. The maximum wind vector length in the figure represents a speed of 45 m s^{-1}.

Figure 5c shows the simulated $\overline{w'w'}$ surface field at 24/0230, while Fig. 5d shows the WSR 57 level 3 and level 5 VIP contours for the same period. Comparison of Figs. 5c and 5d shows generally good agreement between the simulation and observations. While the parameterized convection does not extend as far east as the level 3 VIP contour, the location of the MCV is on the right (eastern) end of the parameterized convective line, and the resolved vertical motion of greater than 1 m s^{-1} and associated precipitation rate maximum extends beyond the end of the parameterized convective line in Fig. 5c.

From 24/0000 to 24/0400, the western portion of the

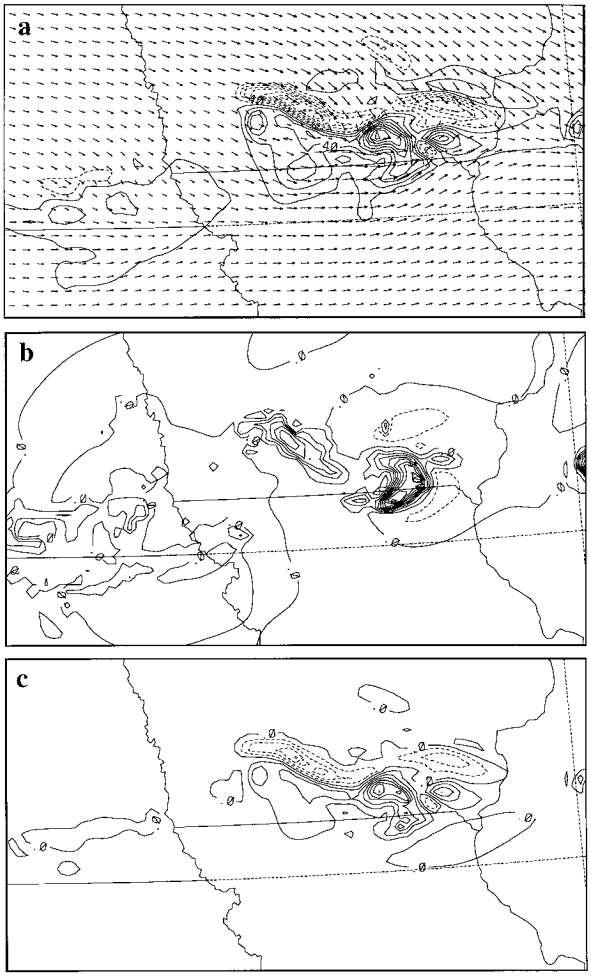

FIG. 11. All plots at time 24/0000 and height of 5220 m ASL. (a) Horizontal winds (max. vector 27 m s^{-1}) and relative vorticity, with a contour level of 2.0×10^{-4} s^{-1}. (b) Vertical velocity, with a contour level of 1.0 m s^{-1}. (c) PV, with a contour level 2 PVU.

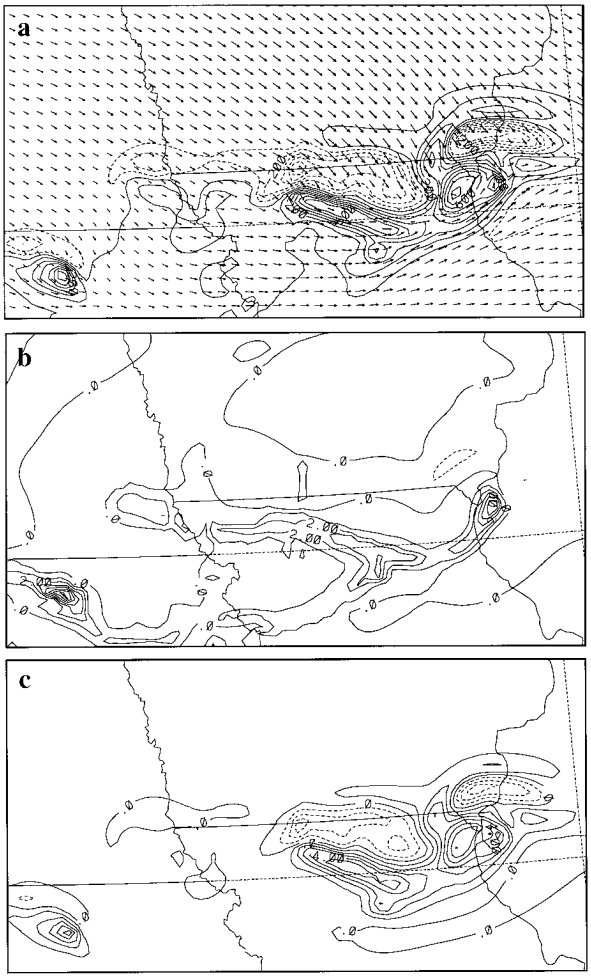

FIG. 12. Same as in Fig. 4 except time 24/0230 and the maximum wind vector in (a) is 28.5 m s^{-1}.

squall line continued to intensify. During the upscale growth of the western extension of the system another vortical circulation began to form over extreme NE Kansas. This mesovortex is evident (Fig. 12, 24/0230) in both the midtropospheric vertical velocity and in the relative vorticity maximum that exceeds 5×10^{-4} s^{-1}. There was also a precipitation maximum associated with this feature, with rain rates exceeding 30 mm h^{-1}. NWS radar summaries (0130–0430) also show a small, yet persistent, area of very strong reflectivity in this region. Radar observations (Fig. 5b,d) show that the strongest convection in the western part of the MCC was oriented parallel to, and south of, the stationary front, giving the convective line a NE–SW orientation. The vertical velocity field over far-eastern Nebraska and Kansas shows well-developed updraft cores, with vertical velocities exceeding 2 m s^{-1}.

By 24/0230 the leading edge in Iowa is well decoupled from the front, though the strong convectively driven circulations have made this frontal region much less distinct. The simulated convection over southern Nebraska and NE Kansas has also started to move away from the front. This time marks the greatest areal extent of parameterized convection. (The greatest convective precipitation rates, however, occurred in the late afternoon, when CAPE values were highest. This diurnal dependence of precipitation rates agrees with the climatology of MCC events in McAnelly and Cotton 1986.) The crescent-shaped vertical velocity maximum in northeastern Missouri in many ways resembles the ''bow-echo'' shape seen in radar observations (Fujita 1978; Schmidt and Cotton 1989; Burgess and Smull 1990) and in simulations (Weisman et al. 1988; Schmidt 1992; Weisman 1992, 1993; Davis and Weisman 1994; SWK). This persistent, southward-propagating bow shape remains apparent in the simulation for several hours, and the shape is still detectable in the midtropospheric vorticity and PV fields at the end of the simulation (not shown).

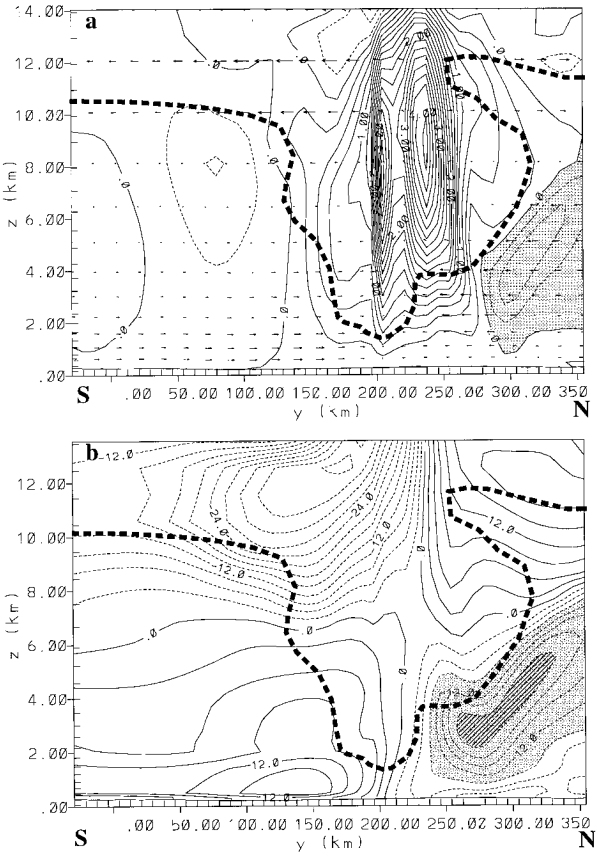

FIG. 13. Both panels at 24/0130. (a) Wind vectors and vertical velocity (contours at 25 cm s^{-1}, shading indicates subsidence). (b) Meridional component of velocity, with contours of 3 m s^{-1} and system-relative rear-inflow jet indicated by the gray shading. The diagonal striping in (b) denotes southward flow $>$ 21 m s^{-1}. The heavy dashed line in both diagrams indicates the approximate outline of the cloud. The location of these cross sections is the same as in Fig. 9. Negative contours in both panels are dashed.

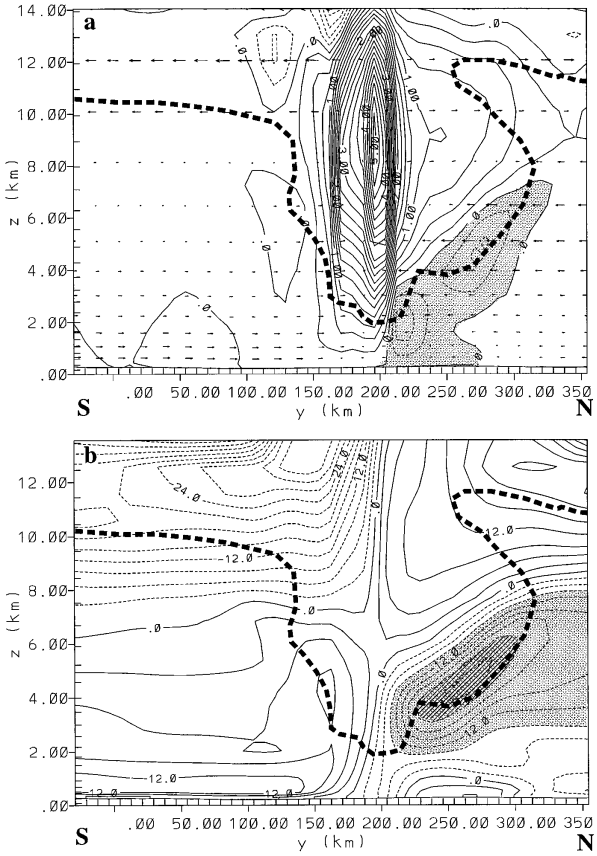

FIG. 14. Same as in Fig. 13 except at time 24/0230.

a. Evolution of the rear-inflow jet

Examination of the wind vector plots in Fig. 4, Fig. 11, and Fig. 12 show an increasingly larger northerly component to the midtropospheric horizontal winds north of the system, with more even pronounced veering in the convective region. Early in the development of the squall line, the midtropospheric flow has a very small meridional component. By 24/0000 there is a distinct meridional storm-induced perturbation, and by 24/0230 the midtropospheric flow is northwesterly over the entire state of Iowa. The existence and evolution of a so-called ''rear-inflow jet'' (RIJ) is a feature common to many squall lines and MCCs. It is well documented in several observational studies (e.g., Smull and Houze 1985,1987a,b; Leary and Rappaport 1987; Johnson and Hamilton 1988; Schmidt and Cotton 1989; Houze et al. 1989) and also appears to be a robust feature in both numerically simulated cases (Zhang and Fritsch 1987,1988; Zhang et al. 1989) and idealized MCS and squall line simulations (Weisman 1992, 1993; Schmidt 1992; Davis and Weisman 1994, SWK).

At 24/0130 a descending RIJ was already well developed (Fig. 13), and an hour later the downdraft had penetrated to the surface (Fig. 14a, 24/0230). Within the (shaded) jet core[5] there are two distinct subsidence maxima, the lower occurring behind the convective line, and another, more rearward and elevated, along the sloping stratiform cloud region. The dipolar structure of mesoscale descent below the stratiform cloud region and ascent within the cloud has been observed in several MCS case studies (e.g., Smull and Houze 1985, 1987a,b; Johnson and Hamilton 1988).

Concurrent with the time the rearward mesoscale downdraft reached the surface behind the convective line, the convective activity began to slowly weaken. Smull and Houze (1987b), who also observed one of the systems in their study to weaken as the descending RIJ reached the surface, theorized that some of the lower θ_e air comprising the jet was entrained from the back

[5] Note that velocity cross sections presented here are *not* system relative, as is the case in the work of Smull and Houze. The gray shading in the N–S cross section corresponds to a contour of $v = -9$ m s^{-1}, which *would* be rear inflow in the relative sense.

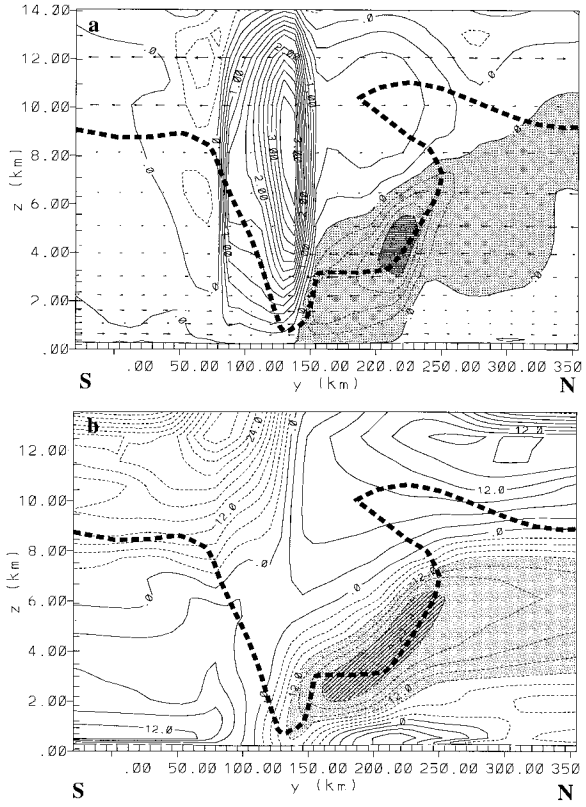

FIG. 15. Same as in Fig. 13 except at time 24/0400. The horizontal hatching in (a) denotes downdrafts in excess of 1 m s^{-1}.

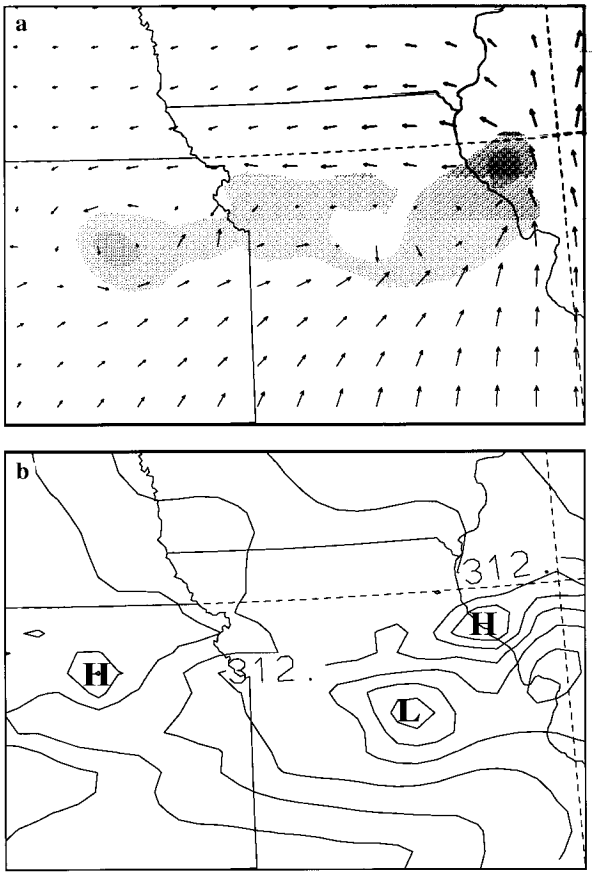

FIG. 16. (a) The storm-relative horizontal winds at 3000 m, 24/0530. The largest wind vector corresponds to a speed of 27 m s^{-1}. The light gray shading denotes areas with relative vorticity greater than 10^{-4} s^{-1}, while the darker shading denotes areas with relative vorticity greater than 4×10^{-4} s^{-1}. (b) The potential temperature θ, also at 3000 m, 24/0530, contour level 1.0K

side into the convective updrafts. This would act to dilute the CAPE and weaken the convection. The θ_e values (not shown) in the lower portion of the simulated RIJ showed a significant depression from surrounding values. The minimum θ_e of 320 K behind the MCC, found initially at about 4.5 km ASL, eventually reached to within 500 m of the surface, near the back of the convective line, lending support to Smull and Houze's hypothesis. At 24/0400, (Fig. 15) about the time of maximum RIJ intensity, the mesoscale downdraft region extended upward from the surface to over 10 km ASL, near the tropopause. Within the RIJ core, downdrafts exceeded 1.25 m s^{-1} and northerly winds extended beyond the front of the convective line. A similar undercutting of the convective updrafts was seen by Smull and Houze (1987b, see their Fig. 11d).

Front-to-rear flows had developed near the surface and above the RIJ in the stratiform region, as seen in Fig. 15b. There is a region of strong divergence near the surface as outflow from the RIJ pushes northward under the stratiform region. The vertical shear in the transition zone between these flow branches exceeds 10^{-2} s^{-1}, in close agreement with Smull and Houze (1987b). A similar three-tiered flow arrangement was seen by Smull and Houze (1985) and Srivastrava et al. (1986).

b. Later evolution of the MCVs

Both of the lower-tropospheric MCVs discussed earlier were still evident at 24/0530 (Fig. 16a) with their associated upper-level vorticity, pressure, and temperature perturbations (not shown) extending almost to the tropopause. The larger, eastern MCV, which had by this time existed for over 8 h, was well behind the weakening convective line, while the smaller and less organized western MCV still contained weak convection. Both MCVs are located near the darker gray, generally circular regions ($\zeta > 4 \times 10^{-4}$ s^{-1}) of roughly 50 km in radius.

Such a vorticity configuration is, at first glance, rather unusual for a squall line. Several simulations of idealized squall lines in sheared environments (Weisman 1992; Davis and Weisman 1994; SWK) show a pattern of what Weisman (1992) terms counter-rotating ''bookend vortices''; a cyclonic vortex to the right (in their cases north, in this case east) of the low-level shear vector, and an anticyclonic vortex to the left (in their

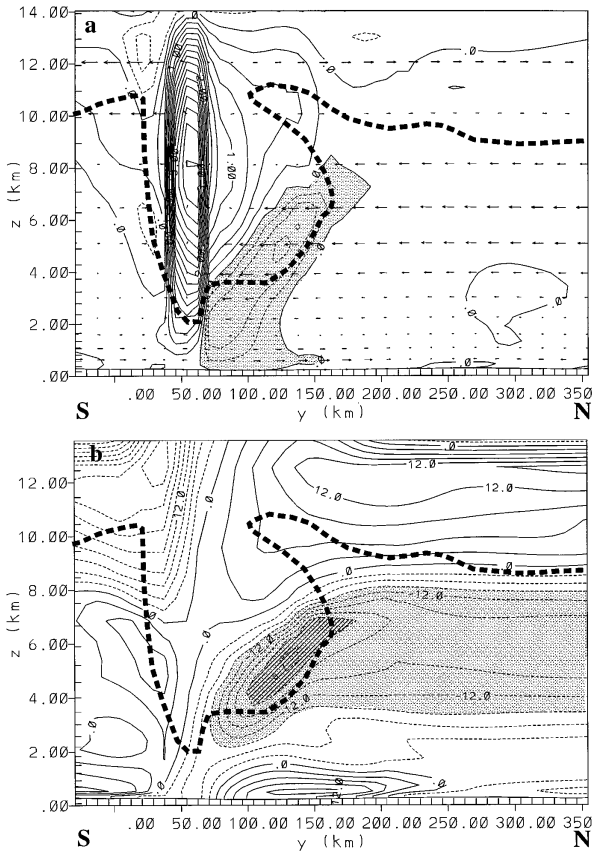

FIG. 17. Same as in Fig. 13 except at time 24/0600.

cases south, in this case west). Here, the vortex to the left of the low-level shear vector (i.e., the MCV in E Kansas) is *cyclonic,* since the vortices evolved in essentially different squall lines that have by this time merged. IR satellite photos (see Fig. 7c of SM) at 24/0600, after the convection has weakened, show a concave shape to the southern edge of the −63°C temperature contour, with a northward deflection along the Kansas–Missouri border. This, and the existence of the persistent, somewhat circular reflectivity maxima mentioned earlier (see Fig. 5f), support the notion that the western end of the observed squall line had, to some degree, developed its own semi-independent mesoscale circulation as occurred in the simulation.

The (system-relative) wind vectors show closed circulations of at least 100 km radius around both MCVs. On the scale of the entire squall line, Fig. 16a shows a systemwide elliptical cyclonic flow encompassing the entire squall line and enhanced by the sharply curved vortical flow on both ends. A similar large-scale elongated and multiple-centered vortical flow was found by Fritsch et al. (1994, see their Fig. 17) in their composite of radar echo motions associated with a weakening MCS. It is interesting to observe that in the older, eastern MCV, the center of the circulation and vorticity maximum are not colocated. A strengthening synoptic-scale anticyclonic circulation around the building high pressure ridge centered in Mississippi was shearing and deforming this vortex as it propagated east. Figure 16b shows that the western MCV had a relatively warm core, in agreement with several MCV observations (e.g., Menard and Fritsch 1989; Fritsch et al. 1994) and modeling studies (Zhang and Fritsch 1987,1988). The older, eastern MCV had a more complex structure, which is difficult to describe as either warm or cold core. The vorticity maximum on the Iowa–Illinois border was colocated with a temperature maximum, but as noted before, the closed circulation extended well beyond the vorticity maximum.

c. Dissipation of the squall line

By 24/0600 the system was dissipating. The system-relative RIJ was no longer descending to the surface (Fig. 17) and the core (> 21 m s^{-1}) was now contained within the stratiform cloud region. The leading-edge updraft zone of vertical velocities greater than 1 m s^{-1} was by now only about 40 km wide while the downdraft maximum within the RIJ was only about 0.8 m s^{-1}, the downdrafts no longer extending upward to the tropopause. While significant N–S divergence was still occurring at the surface where the RIJ intersected the ground, it had weakened considerably in the past 2 h. Further evidence indicative of the weakening system-scale circulation was the dramatic decrease in the divergent southward outflow above 12 km, from a maximum of 33 m s^{-1} at 24/0400 (Fig. 15b) to a maximum of only 24 m s^{-1} just 2 h later.

Figure 5e shows the location of the parameterized convection at 24/0530, which was weakening considerably, and Fig. 5f shows the corresponding NWS WSR57 radar echoes. The location and orientation agree well with the simulation. The strong echo on the eastern Missouri border verifies with the location of the eastern MCV. Even though the convective parameterization is not active there, the model is still simulating updrafts greater than 2.5 m s^{-1} in this region, and producing moderate precipitation. Observations reveal that a new, small convective system, not evident in the radar summary charts or satellite images an hour earlier, had developed in north-central Illinois by 24/0630. Since this was outside the domain of grid 3, the convection was not simulated.

At 24/0730, the parameterized convection had ceased, but the stratiform portion continued to produce light precipitation for about the next 3 h. By 24/1200, all precipitation from the system had ceased. Both MCVs had weakened considerably as they drifted ESE in the mean flow. The upper portion of the eastern MCV continued to elongate due to the shearing action of the developing synoptic-scale flow and the decaying RIJ. While there was no precipitation, upward motions greater than 0.5 m s^{-1} existed at midtropospheric levels in the region of the decaying MCVs. Figure 18 (24/1200)

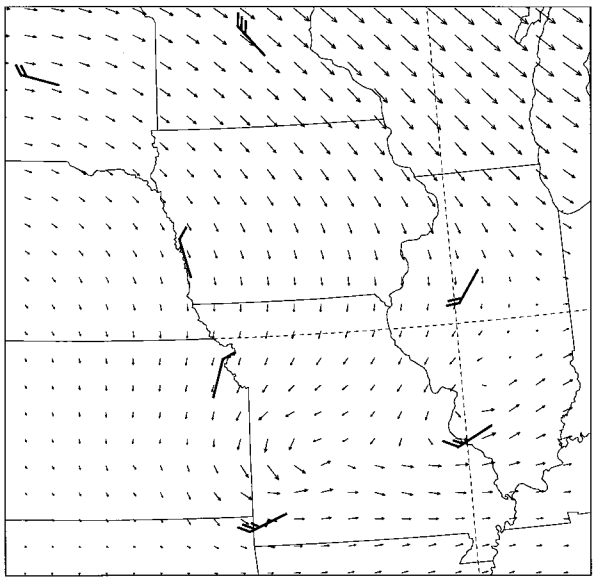

FIG. 18. The model flow field at 5220 m ASL at the end of the simulation, 24/1200. This is the model level closest to the 500-mb level, with a mean pressure of 525 mb. Also plotted in this figure are the 500-mb observed winds (wind barbs) at 24/1200 from the standard NWS soundings. The largest wind vector (N Wisconsin) corresponds to a wind speed of 37 m s^{-1}. Full wind barb flags represent 5 m s^{-1}, half flags 2.5 m s^{-1}.

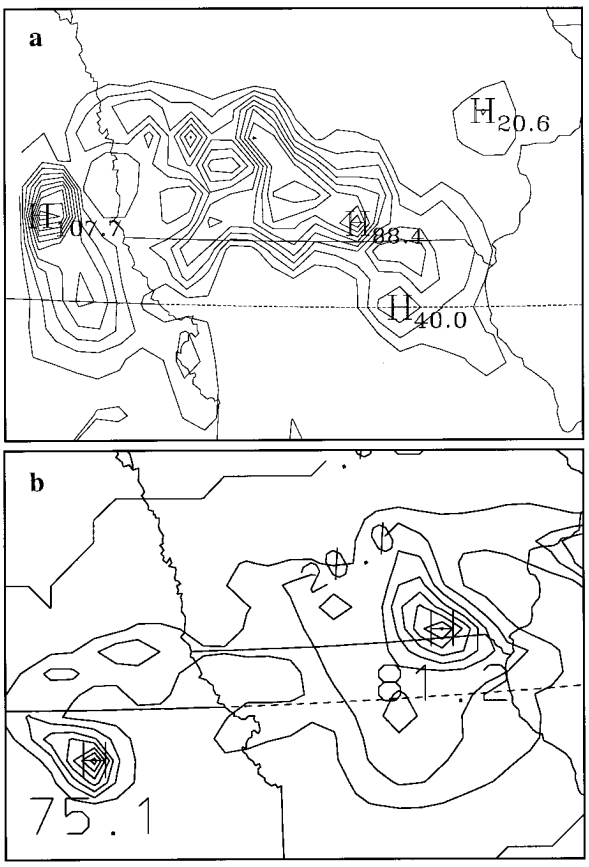

FIG. 19. (a) Observed 24-h precipitation for the period 23/0000→24/0000 CST (23/0600→24/0600 UTC) in mm. (b) Simulated accumulated precipitation for the period 23/1900->24/0600 UTC, also in mm. The contour increment in both figures is 10 mm.

shows the model circulation at 5220 m (horizontal mean pressure 527 mb) and *observed* 24/1200 winds (bold wind barbs) at 500 mb from the standard NMC sounding network. The winds agree quite well in speed and direction, with the notable exception of the Springfield, Illinois sounding value. There, the simulation showed weak northerly winds while the observations had strong southwesterlies. The observed wind field likely was locally influenced by the convection that had occurred in central Illinois for the past several hours. This convection was not simulated by the model.

Though this system occurred outside the PRE-STORM network, there were PRE-STORM research aircraft flights through the system in the period from 24/0900 to 24/1300. The daily operations summary from the field project (Meitín and Cunning 1985) noted that the two aircraft encountered a warm-core vortical circulation at 10 000 ft. (3050 m) over east-central Missouri at around 24/1030. This agrees fairly well with Fig. 16, (3000 m) valid at 24/1030. Meitín and Cunning further state that the circulation did not seem to be found at 15 000 ft (4600 m) by the other aircraft at that time. Johnson and Bartels (1992) comment that the vortex was evident in the standard 500-mb NMC analysis for 24/1200. Examination of the wind barbs alone in Fig. 18, obtained from the NMC analysis referred to by Johnson and Bartels, does seem to indicate a closed cyclonic circulation over Missouri. The simulated winds (wind vectors), which are more resolved, show a much more complex circulation, though obviously there exists meteorologically significant positive vorticity over the post-MCC region. Brody (1987) detected a ''distinct comma shape, indicating an upper vorticity maximum had formed.'' This comma feature, seen on the visible satellite image at 24/1230, is about 100 km east of the simulated 24/1200 midtropospheric vertical velocity maximum.

Figure 19a contains a plot of observed 24-h precipitation totals for the period 23/0000 to 24/0000 CST (23/0600 to 24/0600 UTC) obtained from National Climatic Data Center hourly and 3-hourly precipitation databases and from special storm spotter reports. Figure 19b shows the simulated accumulated precipitation for the period (23/1900 to 24/0600 UTC). Radar summary charts and the hourly precipitation data (only sparsely available) indicate that most of the observed precipitation above a line 100 km north of, and parallel to, the Iowa border fell in the morning of 23 June, before convection was allowed in the simulation. South of that line, the simulation and observations agree fairly well. The simulated maximum (81.2 mm) just north of the Iowa border is about 50 km east of the corresponding observed maximum (88.4 mm), which agrees with the

50 km eastern offset of the developing MCV at 23/2230 relative to the observed tornadoes, large hail and very heavy rainfall at the same time. The smaller maxima (30+ mm simulated and 40 mm observed) on the 40th parallel in NE Missouri are almost collocated. The precipitation maximum (75.1 mm) in NE Kansas is about 125 km south of the corresponding maximum (107.7 mm) in SE Nebraska.

This larger offset suggests that the model did a relatively poor job with the western portion of the MCC. The simulated meso-α-scale midlevel vertical motion field over eastern Nebraska in the late afternoon was slightly negative, in contrast to the slightly positive w values (Fig. 8a) seen over south-central Iowa at the same time. The subsidence and associated adiabatic warming acted to suppress the parameterized convection in Nebraska when CAPE values were highest in the late afternoon. Though the parameterization was active here, it only produced a local precipitation maximum slightly greater than 20 mm. By the time the parameterized convective line in NE Kansas had intensified around 24/0130, the CAPE values had dropped to less than 2000 J kg^{-1} and the subsidence induced by the storm in Iowa and Missouri was considerable. Still, the distinct bimodal E–W distribution of precipitation in both the observed and simulated fields supports the hypothesis that two distinct mesoscale convective lines were coexisting under the large cloud shield seen in satellite images and model condensate fields. Outside these maxima, the model seems to have been consistent in underpredicting the precipitation by about 30%–40%.

6. Discussion

a. MCV formation

Several observational studies indicate that MCV development occurs during the mature to dissipating stage of the MCC. Johnson et al. (1989) and Johnson and Bartels (1992) observed an MCV extending from about 3 km to over 8 km in a mature-to-decaying MCS. Menard and Fritsch (1989) observed a very large MCV at the 700- and 500-mb levels imbedded in a dissipating MCC. These studies and others (e.g., Smull and Houze 1985, 1987a; Leary and Rappaport 1987; Fritsch et al. 1994) relate the formation of the MCV to the development of the stratiform precipitation region commonly found in mature and decaying MCSs.

Similar results are also obtained in numerical studies of mesoscale convection. Zhang and Fritsch (1988), simulating the case analyzed by Menard and Fritsch, found the MCV to develop in the dissipating stage, with a vorticity maximum located between 600 and 700 mb. In their idealized three-dimensional horizontally homogeneous squall line simulations, SWK found the development of a midlevel MCV after 6 h of convection. After about 6–8 h of parameterized stratiform diabatic heating, the balanced model simulations of Jiang and Raymond (1995) developed a cyclonic mesovortex in the stratiform region extending vertically from 4 to 8 km.

One of the interesting results of the 23–24 June simulation is the rapid evolution of the MCV at relatively low levels over south-central Iowa. Evidence for early MCV development does exist in a few observations and simulations of squall lines. Brandes (1990) found evidence in profiler data of a closed vortical circulation below 4 km within about 3 h of squall line formation and suggested that an existing vortex could be a precursor. Verlinde and Cotton (1990) found evidence of a relatively short-lived cyclonic vortex in dual-Doppler radar observations of a developing MCC. Other studies (e.g., Zhang et al. 1989) have found pre-existing vortices that were amplified by the convective and mesoscale storm-driven circulations. Using a strong low-level shear profile and no coriolis force in a domain with ''mirror'' lateral boundary conditions, Weisman (1993) simulated bow-echo type squall lines which developed ''bookend vortices,'' that is, counter-rotating vortices at the ends of the convective line. These features were well established within 180 min of simulated resolved convection. Such results indicate that there are perhaps several mechanisms that produce the vortices associated with mesoscale convection.

To address these mechanisms, consider the vertical vorticity equation in Eulerian form

$$\frac{\partial \zeta}{\partial t} = \underbrace{-\mathbf{V}\cdot\boldsymbol{\nabla}_h\zeta}_{\substack{\text{hor}\\ \text{adv}\\ \text{(a)}}} \underbrace{- w\frac{\partial \zeta}{\partial z}}_{\substack{\text{vert}\\ \text{adv}\\ \text{(b)}}} \underbrace{(\zeta + f)\delta_h}_{\substack{\text{conv/}\\ \text{stretch}\\ \text{(c)}}}$$

$$\underbrace{- \left(\frac{\partial w}{\partial x}\frac{\partial \upsilon}{\partial z} - \frac{\partial w}{\partial y}\frac{\partial u}{\partial z}\right)}_{\substack{\text{tilting}\\ \text{(d)}}}$$

$$\underbrace{+ \rho^{-2}\frac{\partial(\rho, p)}{\partial(x, y)}}_{\substack{\text{baroclinic}\\ \text{(e)}}} + \underbrace{\mathbf{k}\cdot(\boldsymbol{\nabla} \times \mathbf{F}/\rho)}_{\substack{\text{friction}\\ \text{(f)}}}, \qquad (1)$$

where u, υ, and w are wind components in x, y, and z directions, p and ρ are pressure and density, δ_h represents the horizontal divergence, $\boldsymbol{\nabla}_h$ the horizontal gradient operator, and $\mathbf{F}$ the vector frictional force. (Note that the baroclinic term is very small in this context.) As in Davis and Weisman (1994) the Eulerian framework is used since this avoids the difficulty of choosing ''representative'' trajectories in this complex flow regime.

Weisman (1993) suggests that tilting of the large *ambient* horizontal vorticity [term d of (1)] by downdrafts was responsible for the production of bookend vortices. In discussing their fully three-dimensional squall line simulations, Davis and Weisman (1994) attribute MCV development to tilting of *baroclinically generated* (vs ambient) horizontal vorticity in the ascending front-to-rear circulation and descending RIJ, noting that the more

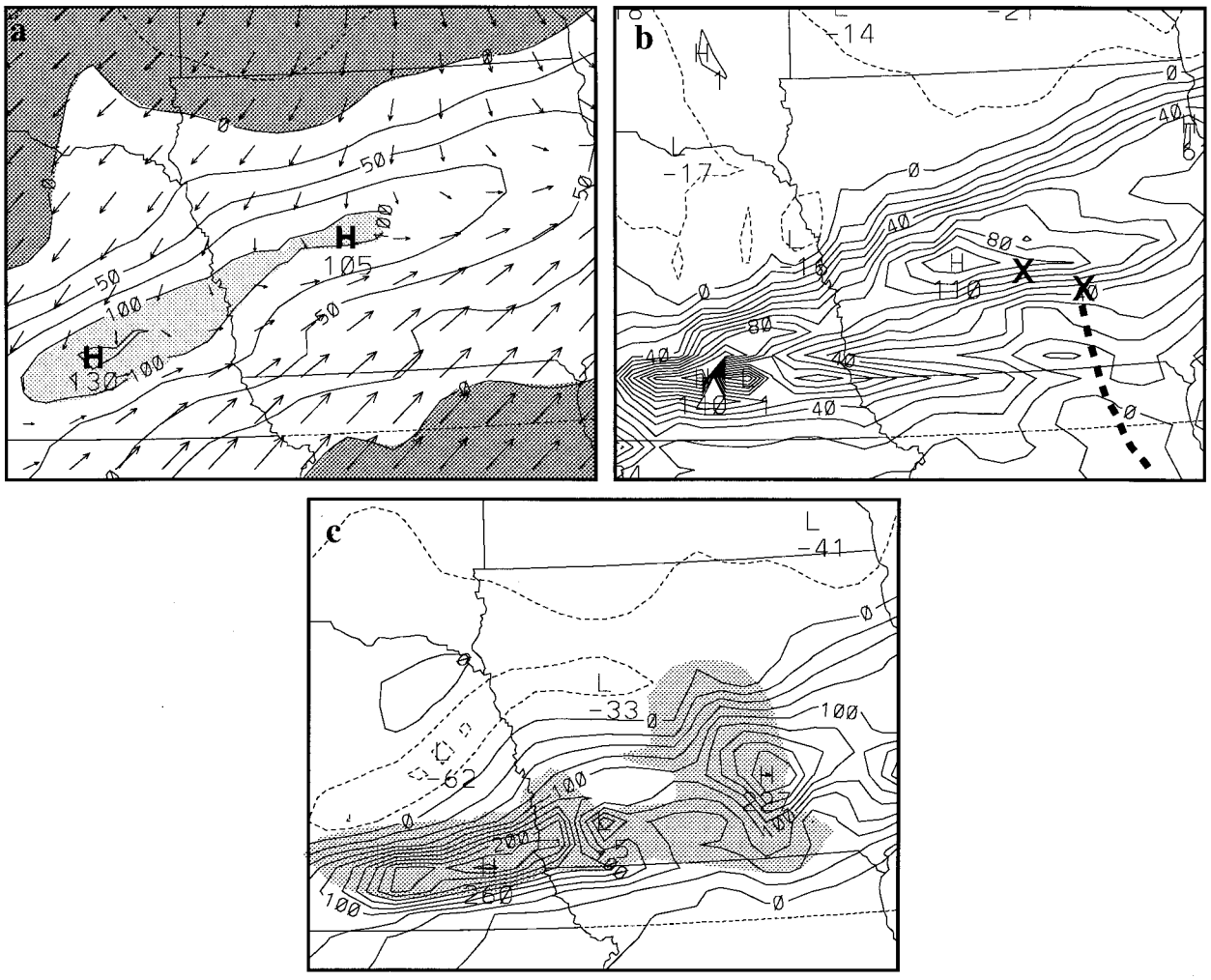

FIG. 20. (a) Relative vertical vorticity at 270 m, 23/1900, with a contour increment of 2.5×10^{-5} s^{-1}. The dark gray shading indicates negative vorticity and the light gray shading indicates relative vorticity greater than the local planetary vorticity, *f*. (b) Convergence/stretching of absolute vorticity, also at 270 m, 23/1900, contour increment of 1×10^{-9} s^{-2}.(c) Relative vertical vorticity at 270 m, 23/2130, with a contour increment of 2.5×10^{-5} s^{-1}. The shaded region indicates the average convergence/stretching of vorticity greater than 1×10^{-8} s^{-2}. The average was computed vertically over the lowest 1 km of the domain for the 90-min period 23/2000→23/2130. (At any given time, the maximum values approached 10^{-7} s^{-2} locally, but this was lost in the averaging process.)

rapidly generated bookend vortices of Weisman (1993) developed in an environment with at least twice the low-level shear used in their experiments.

This distinction is important to the timescale of development. The explanations proposed both by Davis and Weisman (1994) and SWK invoke the vertical motion of mesoscale flow branches and baroclinically generated horizontal vorticity. These features are largely manifestations of evaporative cooling, especially from precipitation produced in the stratiform region, and typically develop only after several hours of convection. The importance of the stratiform region to MCV production is also supported by Leary and Rappaport (1987) and Johnson and Bartels (1992) and the modeling studies of Zhang and Fritsch (1988). In other modeling studies (Zhang and Fritsch 1987; Chen and Frank 1993), a midlevel shortwave propagating in the ambient flow was found to further enhance the diabatic processes in initiating and amplifying a mesoscale vortex.

In light of the foregoing discussion it is worthwhile to investigate how the vortex over Iowa organized so rapidly in the present simulation, as evidenced, for example, by the vorticity and wind fields at 23/2230 seen in Fig. 6. Figure 20a (23/1900, previous to any convection) shows the relative vorticity at 270 m. The lightly shaded region, where the absolute vorticity exceeds 2*f*, lies just along and to the south of the stationary front at the surface (see Fig. 2) and is embedded in a larger-scale field of anticyclonic relative vorticity under the synoptic ridge. Figure 20b shows the convergence of absolute vorticity [term c in (1)] also at 23/1900, averaged over the lowest 1 km of the domain. The two

maxima, which correlate well with the ζ maxima in Fig. 20a, have values exceeding 10^{-8} s^{-2}, a rate that would increase the vorticity by a value of f in less than 3 h. (Interestingly, both MCVs in the simulation developed just to the south of the two ζ maxima in Fig. 20a.) At this time convergence/stretching exceeded the other terms by at least an order of magnitude. The northernmost X in Fig. 20b represents the location of the ζ maximum at 23/2030, and the southernmost X locates the maximum at 23/2130. The dashed line shows the path of the vortex once the circulation became closed, sometime between 23/2130 and 23/2200. This environment is in marked contrast to that of Weisman (1993) where the absolute vorticity was zero and the f-plane simulations of Davis and Weisman (1994) and SWK where the initial relative vorticity field was neutral.

Figure 20c (23/2100) displays ζ at 270 m, 1.5 h after the initiation of convection associated with the squall lines. The vorticity in and just behind the squall line has increased significantly and is well correlated with the enhanced spatially and temporally averaged ζ convergence (shaded region). Though the other terms in the vorticity equation had significant maxima and minima at any given time and height, the time average showed little coherent trend. (At any given time, the maximum values approached 10^{-7} s^{-2} locally, but this was lost in the averaging process.) Tilting and vertical advection were of secondary significance and both these terms gave mostly negative tendencies on the average. At 23/2230, an hour later, the relative vorticity had almost doubled again, exceeding $4f$ and yielding the circulation at 270 m seen in Fig. 6b. After this time the vorticity at this level increased only slowly, with significant cancellation between the fairly large convergence and vertical advection terms.

At higher levels (between about 1500 and 3500 m) the apparent source of the enhanced vorticity is much less evident. Above about 1 km, the updraft strength increases dramatically, and tilting of horizontal vorticity becomes much more significant. Figure 21 shows vorticity tendencies averaged vertically in the layer from 1 km to 2.5 km AGL and averaged horizontally across the MCV. At early times, vertical advection dominated, with tilting the next dominant term. Once the vortex was established, these three terms were in a state of approximate cancellation, though the magnitude of each term varied widely in both time and space.

The development of large vorticity values first below 1 km and the importance early on of vertical advection above 1 km suggests that the vortex first developed near the surface as a result of convergence of large ambient vorticity, which was consequently advected upward.[6]

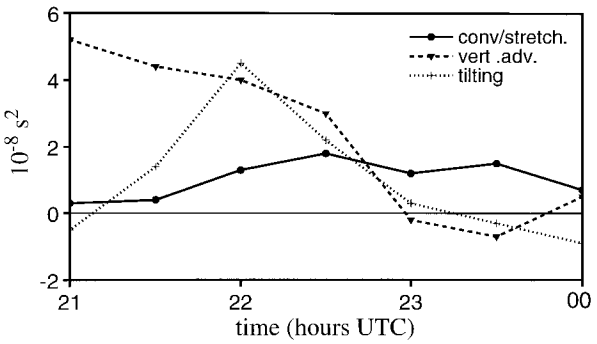

FIG. 21. Vorticity tendencies (10^{-8} s^{-2}) vertically averaged from in the layer from 1 km to 2.5 km AGL and horizontally averaged across the MCV. These individual tendencies correspond to terms in Eq. (1): (*b*) vertical advection, (*c*) convergence/stretch, (*d*) tilting. The values were computed at half-hour intervals from 23/2100 to 24/0000.

Concurrently, tilting of ambient and storm-generated horizontal vorticity was occurring above 1 km, where the ambient vertical vorticity was considerably less. With both vertical advection and tilting producing a source of enhanced vorticity, the substantial convergence above 1 km could then operate efficiently to spin up and maintain the vortex. Above about 4000 m, the production (in an Eulerian sense) of positive vorticity was still very large, but the shearing action of the strong westerlies (i.e., differential horizontal advection of ζ) strongly deformed the vorticity field, preventing development of a closed circulation.

This proposed mechanism is similar to that discussed in Zhang et al. (1989). In their MCS simulation, a pre-existing meso-α-scale cyclonic vortex is seen in the lowest 100 mb of the atmosphere. They attribute the deepening and intensification of the mesovortex to stretching by diabatically driven circulations. At a much smaller scale, recent very high-resolution numerical simulations of two different tornadic thunderstorms (Grasso 1995; Grasso and Cotton 1996) found tornado vortex generation to also progress upward in a manner similar to that discussed here.

b. Along-line banded vorticity structure

Another intriguing feature seen in the later period of the simulation is the banded vorticity pattern oriented parallel to the squall line. Such vorticity banding has been observed in the 10–11 June PRE-STORM MCS, both in Doppler radar studies (Biggerstaff and Houze

[6] A reviewer noted that if the frictional forces and baroclinic terms are neglected and the Boussinesq approximation is made, 1) may be rewritten as $\partial\zeta_z/\partial t = -\nabla_h \cdot \mathbf{Y}$ with $\mathrm{Y} = \mathbf{V}_h\zeta_h - \zeta_h w$ a "generalized" vorticity flux and ζ_z the vertical absolute vorticity. In this flux divergence form, the local tendency of vertical vorticity is independent of a vertical flux divergence. Note, however, that the vertical advection term $w\partial\zeta_z/\partial z$ in (1) has been replaced by $-w(\nabla_h \cdot \zeta_h)$, a consequence of $\nabla \cdot (\nabla \times \mathbf{V}) \equiv 0$. Vertical advection of vorticity is still implicitly represented in this flux divergence form, but appears as the vertical transport of the horizontal convergence of horizontal vorticity.

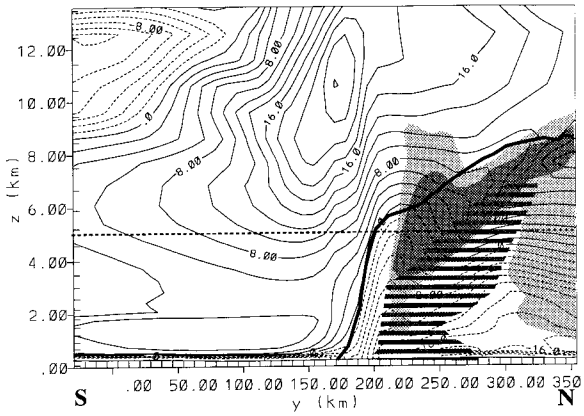

FIG. 22. Contours of the E–W (u) component of the system-relative wind at 24/0230 with a contour level of 2 m s^{-1}. The light gray shading denotes the area where relative vorticity is negative, while the darker gray indicates negative PV. The horizontal bars show the region of subsiding motion. The heavy dark line locates the zero contour of meridional velocity (not storm relative). This cross section has the same location as Fig. 14, and the horizontal dashed line locates the level of the horizontal cross section in Fig. 12.

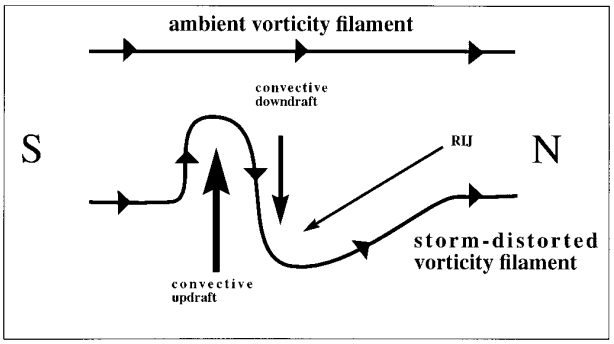

FIG. 23. A schematic illustration of how a vorticity filament, initially almost horizontal, becomes distorted (tilted) by the MCS generated vertical motion field (similar to Biggerstaff and Houze 1991b, Fig. 8).

1991a,b) and MCS simulations (Zhang et al. 1989) of that case. Biggerstaff and Houze, who saw relative vorticity $\zeta < -3 \times 10^{-4}$ s^{-1} in a band along the transition zone (Smull and Houze 1987a) just behind the updraft cores, concluded that tilting of horizontal vorticity was largely responsible for the banding in their case. Biggerstaff and Houze (1989) state that midlevel vorticity banding in MCSs was apparently undocumented prior to their study, which suggests that such features are perhaps atypical in the MCS population, although Schmitt and Cotton (1989) showed midlevel streamlines that indicated a similar anticyclonic band.

A very similar feature is seen here in the 23–24 June simulation. Even in the earliest stages of squall line development (Fig. 4a, 23/2100) a very narrow band of negative relative vorticity $\zeta < -2 \times 10^{-4}$ s^{-1} is found behind the updraft cores along the Iowa–Misssouri border. Three hours later, (Fig. 11a) the bow-shaped line in SE Iowa has developed a wider band of negative relative vorticity, with $\zeta < -6 \times 10^{-4}$ s^{-1}. By 24/0230 (Fig. 12a) this feature, though weaker, is still evident, and a positive band has developed to the rear of the MCC. Figure 12a looks quite similar to Fig. 3a (550 mb) of Biggerstaff and Houze (1991b). As expected, this banding is also evident in the PV fields, [see panel (c) in Fig. 4, Fig. 11, and Fig. 12], with the $\zeta = -1 \times 10^{-4}$ contour agreeing with the transition from positive to negative PV values. Panels (c) and (d) in Fig. 9 show N–S cross sections of ζ and P, respectively, at 24/0230. Comparison with Fig. 14 strongly suggests that the RIJ is fundamental to the formation and orientation of the negative banding seen in these cross sections.

Examination of Fig. 22 (24/0230) further illustrates this point. The contours of zonal velocity are strongly deformed in the region of the RIJ, which is advecting the zonal momentum downward and southward. The relative vorticity is very large in the convective updrafts. Note that the locations where $\partial u/\partial y$ changes sign correlate well with the boundary between positive and negative relative vorticity (light gray in the figure), indicating that the vorticity is largely determined by horizontal shear of u. Further, $\partial u/\partial y$ is largest just along the southern extent of the downdraft region (left side of horizontal bars). Moving north, the vorticity again becomes positive near the core of the RIJ.

It is useful to also consider this banded structure from the standpoint of the vorticity budget. Noting that the midlevel ambient horizontal vorticity vectors in their case had a significant component normal to the squall line, pointing toward the rear, Biggerstaff and Houze (1991b) appealed to the tilting of horizontal vorticity to explain the banded vorticity structure in their case. Figure 23 schematically illustrates the distortion, by tilting, of a representative vorticity filament in the region of the convective updraft–downdraft couplet and descending rear inflow. This figure may be considered, in the current case, as a projection of the (horizontal) vorticity filaments onto a vertical N–S plane bisecting the squall line near its midpoint. (In the 10–11 June, 1985 case of Biggerstaff and Houze, the convective line had a north–south orientation. Therefore, Fig. 23 would be appropriate in their case if the labels south and north were replaced by east and west, respectively.) The perturbed filament in the bottom half of the diagram is tilted steeply upward, then downward by the combined action of convective downdrafts and the RIJ. To the rear of the system, the filament again tilts upward into its undisturbed position. Biggerstaff and Houze state that tilting *must* be involved since, neglecting baroclinic and frictional effects, the vertical vorticity (in the Lagrangian sense) can change sign only by tilting. Convergence/stretching acts only to concentrate or disperse vorticity filaments.

The same mechanism seems to be acting in this simulation. Figure 24a shows a vertical profile of the horizontal components of vorticity ahead (south) of the

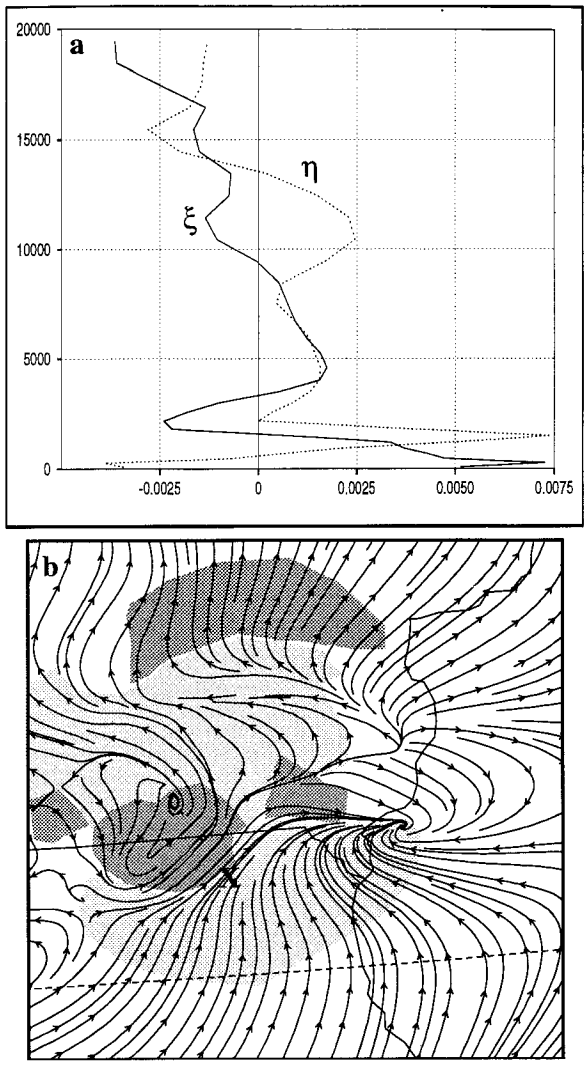

FIG. 24. (a) Vertical profile of the horizontal components of vorticity (ξ zonal and η meridional) at 24/0000 for the location marked by the **X** in Fig. 24b. This may be considered as representative of the background horizontal vorticity ahead of the squall line. (b) Horizontal vorticity filaments at 5220 m and 24/0000. The light gray shading indicates negative tilting of horizontal vorticity and darker gray indicates tilting in the positive sense.

squall line. Between about 3 km and 8 km, the profile is quite typical of the large-scale environment in which the MCS developed. At the height of 5220 m (the dashed line in Fig. 22), both the zonal (ξ) and meridional (η) components of vorticity are positive and of similar magnitude, near 2×10^{-3} s^{-1}, or about 20 times larger than *f*. Therefore, the total vorticity vector is almost horizontal, and pointed to the northeast, giving a substantial component of horizontal vorticity normal to the squall line as depicted in the schematic diagram.

Figure 24b shows midtropospheric horizontal vorticity vectors at 24/0000. A plot of horizontal vorticity filaments at 23/1900 (not shown) just previous to any convection was quite smooth and relatively featureless, resembling the structure seen in the extreme northern and southern portions of Fig. 24b. After several hours it is obvious that the horizontal vorticity had been dramatically distorted in the region of the MCC. Figure 24b reveals a considerable region of negative tilting of undisturbed vorticity in the midtropospheric subsidence region well ahead of the system and another large region of positive tilting of ambient vorticity well behind the convective line. The gross distortion of the horizontal vorticity filaments within the system, however, shows that *the tilting mechanism is operating on a strongly modified vorticity field bearing little relation to ambient conditions, and caution must be used in applying theories that invoke tilting of environmental vorticity.*

The overall tilting pattern seen in Fig. 24b remains almost unchanged, with respect to the MCC, for the period from 24/0000→24/0300 and is fairly representative of the tilting trend throughout the 4000 to 8000 m layer, suggesting that this mechanism is quasi-steady state. Convergence/stretching is also acting on the lowest 7 km of the system as a whole, with a magnitude typically similar to that of tilting. Meridional convergence is especially strong, acting to amplify the tilting tendencies seen in Fig. 24b and meridionally contract the vertical vorticity perturbation.[7] This is consistent with the vertical vorticity field seen in Fig. 11b.

7. Summary and concluding remarks

In this paper, observations and a numerical simulation of a large midlatitude MCC are presented and discussed. The MCC, which occurred over the central United States 23–24 June 1985 was spawned in an environment that in many ways typifies that favored for MCC genesis, positive low-level temperature, and moisture advection under the periphery of a synoptic-scale midtropospheric ridge. The near-surface conditions, characterized by large CAPE and positive mesoscale vertical motion values, were typical of that seen south of a shallow stationary front during the summer months.

The multiply nested-grid simulation agreed reasonably well with surface, upper-air, and satellite observations and ground-based radar plots. It produced a typical structure consisting of a leading line of vigorous convection, and a trailing region of less intense stratiform rainfall. Also simulated in the lower troposphere were two mesoscale convectively induced vortices, features frequently associated with MCCs and MCSs. Several other ubiquitous MCC circulations were also simulated: a divergent cold pool in the lower troposphere, midlevel convergence coupled with a relatively cool descending RIJ and relatively warm updraft structure, and a cold divergent anticyclone in the tropopause region.

[7] It should be emphasized that the vorticity-budget approach to understanding the evolution of circulations in such a complex and evolving system as a MCC is qualitative and heuristic.

Two fairly atypical aspects of the simulation were evaluated in the context of vorticity dynamics. While MCVs are often found in mature and dissipating MCCs, the development of closed mesovortices during upscale growth is evidently much less common. The simulated MCV on the eastern end of the convective line was shown to have rapidly developed in a narrow band of large relative vorticity located parallel, and to the south of, the stationary front. Convectively induced convergence enhanced the already considerable low-level convergence of vorticity, rapidly spinning up the vortex below 1500 m. Tilting, convergence/stretching, and vertical advection all acted to enhance the vorticity above this level, producing a long-lived storm-relative closed circulation extending from a few hundred meters AGL to about 4000 m. The diabatic effects generally associated with MCV generation in the mature and dissipating stages of MCCs were also at work in this simulation and likely contributed to the longevity of the vortical circulation.

The midlevel banding of positive and negative vertical vorticity parallel to the leading convective line was another rather anomalous element of the simulation. This structure was shown to be explainable both from the standpoint of momentum transport by the RIJ and convective updrafts and from a complementary analysis of the vorticity budget. The explanation presented here is in most respects similar to that derived from observations of similar banding in MCSs.

Several intriguing aspects of the simulation have yet to be explored. The sloping nonconvective mesoscale circulations and associated negative absolute vorticity regions suggest that conditional symmetric instability (CSI) may be occurring. Recent work (e.g., Blanchard 1994) suggests that inertial instability at upper levels may also enhance the growth of MCSs. These will likely be areas of future work.

Part II of this work will present a complementary approach to the analysis presented here. It will be shown that the vorticity viewpoint in this paper is consistent with the evolution of balanced flow in MCSs, and that the circulations seen in this MCC simulation are, to a great degree, contained within the nonlinear balance approximation, the related balanced omega equation, and the PV as analyzed from the numerical model results.

Acknowledgments. The authors are grateful for the thoughtful advice and encouragement offered from several parties, in particular, Drs. Wayne Schubert and Michael Montgomery and Rolf Hertenstein. Thanks are also given to Dr. Hongli Jiang and Ray McAnelly for their careful and constructive reviews of this manuscript. We would also like to thank Dr. J. M. Fritsch and two anonymous reviewers for their insightful comments and suggestions, which helped to make this a more informative and focused paper. This work was supported by the National Science Foundation through Grant ATM-9118963.

APPENDIX

Level 2.5w Convective Adjustment Scheme

The level 2.5w convective adjustment scheme (Weissbluth and Cotton 1993) was designed for use with grid sizes from 5 to 50 km, a scale at which many convective parameterization schemes are not applicable. The level 2.5w scheme incorporates an extension of the Mellor and Yamada (1974) level 2.5 turbulence closure based on vertical velocity variance, $\overline{w'w'}$, rather than turbulence kinetic energy (TKE). In this scheme, $\overline{w'w'}$ is treated as a prognostic variable that is advected by the model's resolved winds.

This convective parameterization consists of two parts; a microscale vertical diffusion scheme that controls subgrid-scale vertical mixing, and a cumulus-scale updraft/downdraft component that is driven by a one-dimensional cloud model. In the absence of deep convection, the vertical diffusion component provides tendencies to the prognostic variables proportional to gradients in their subgrid-scale vertical fluxes. When the scheme has determined that deep convection is present, additional tendencies are fed into the host model. The one-dimensional cloud model produces a vertical profile for each column, and at each time step, tendencies are computed for the temperature and the various microphysical species. In this manner, the host model is ''nudged'' toward the evolving one-dimensional cloud profile on a timescale determined by, among other things, cloud-core fractional coverage of updrafts and downdrafts, the profile of $\overline{w'w'}$, and differences between in-cloud and environmental values of the variable under consideration.

Another characteristic feature of the parameterization is its ability to directly provide a source of hydrometeors for the host model, in contrast to other schemes (e.g., Kuo 1965, 1974; Arakawa and Schubert 1974; Fritsch and Chappel 1980), which simply moisten the host model, requiring nucleation processes to occur there. A similar approach has been implemented in a modified version of the Kain and Fritsch (1990) convective parameterization scheme (Zhang et al. 1994).

REFERENCES

Arakawa, A., and W. H. Schubert, 1974: Interaction of a cumulus cloud ensemble with the large-scale environment. Part I. *J. Atmos. Sci.,* **31,** 674–201.

Augustine, J. A., and K. W. Howard, 1988: Mesoscale convective complexes over the United States during 1985. *Mon. Wea. Rev.,* **116,** 685–701.

——, and ——, 1991: Mesoscale convective complexes over the United States during 1986 and 1987. *Mon. Wea. Rev.,* **119,** 911–919.

Barnes, S. L., 1973: A technique for maximizing details in numerical weather map analysis. *J. Appl. Meteor.,* **3,** 396–409.

Bartels, D. L., and R. A. Maddox, 1991: Midlevel cyclonic vortices generated by mesoscale convective systems. *Mon. Wea. Rev.,* **119,** 104–118.

Biggerstaff, M. I., and R. A. Houze Jr., 1991a: Kinematic and pre-

cipitation structure of the 10–11 June 1985 squall line. *Mon. Wea. Rev.*, **119,** 3034–3065.

——, and ——, 1991b: Midlevel vorticity structure of the 10–11 June 1985 squall line. *Mon. Wea. Rev.*, **119,** 3066–3078.

Blanchard, D. O., 1994: Jet-induced inertial instabilities and the growth of mesoscale convective systems. Dept. of Atmos. Sci. Paper No. 571, 190 pp. [Available from Department of Atmospheric Science, Colorado State University, Fort Collins, CO 80523-1371.]

Brandes, E. A., 1990: Evolution and structure of the 6–7 May 1985 mesoscale convective system and associated vortex. *Mon. Wea. Rev.*, **118,** 109–127.

Brody, F. C., 1987: An excessive rainfall event caused by the interaction of a convectively-induced upper-level vort max, a front, and an outflow boundary. *Natl. Wea. Dig.*, **11,** 37–41.

Burgess, D. W., and B. F. Smull, 1990: Doppler radar observations of a bow echo associated with a long-track severe windstorm. Preprints, *16th Conf. on Severe Local Storms*, Kananaskis Park, Alberta, Canada, Amer. Meteor. Soc., 203–208.

Chen, C., and W. R. Cotton, 1983: A one-dimensional simulation of the stratocumulus-capped boundary layer. *Bound.-Layer Meteor.*, **25,** 289–321.

Chen, S. S., and W. M. Frank, 1993: A numerical study of the genesis of extratropical convective mesovortices. Part I: Evolution and dynamics. *J. Atmos. Sci.*, **50,** 2401–2426.

Cotton, W. R., M.-S. Lin, R. L. McAnelly, and C. J. Tremback, 1989: A composite model of mesoscale convective complexes. *Mon. Wea. Rev.*, **117,** 765–783.

Davies, H. C., 1983: Limitations of some common lateral boundary schemes used in regional NWP models. *Mon. Wea. Rev.*, **111,** 1002–1012.

Davis, C. A., and M. L. Weisman, 1994: Balanced dynamics of mesoscale vortices in simulated convective systems. *J. Atmos. Sci.*, **51,** 2005–2030.

Fritsch, J. M., and C. F. Chapell, 1980: Numerical prediction of convectively driven mesoscale pressure systems. Part I: Convective parameterization. *J. Atmos. Sci.*, **37,** 1722–1733.

——, J. D. Murphy, and J. S. Kain, 1994: Warm-core vortex amplification over land. *J. Atmos. Sci.*, **51,** 1780–1807.

Fujita, T. T., 1971: Proposed characterization of tornadoes and hurricanes by area and intensity. SMRP Res. Paper No. 91, 87 pp. [Available from Department of Geophysical Sciences, University of Chicago, Chicago, IL 60637.]

——, 1978: Manual of Downburst identification for Project Nimrod. SMRP Res. Paper No. 156, 104 pp. [Available from Department of Geophysical Sciences, University of Chicago, Chicago, IL 60637.]

Grasso, L. D., 1995: Numerical simulation of the May 15 and April 26,1991 tornadic thunderstorms. Dept. of Atmos. Sci. Paper No. 596, 202 pp. [Available from Department of Atmospheric Science, Colorado State University, Fort Collins, CO 80523-1371.]

——, and W. R. Cotton, 1996: Numerical simulation of the May 15, 1991 Laverne, Oklahoma tornado. Preprints, *18th Conf. on Severe Local Storms*, San Francisco, CA., Amer. Meteor. Soc., 278–282.

Hoskins, B. J., M. E. McIntyre, and A. W. Robertson, 1985: On the use and significance of isentropic potential vorticity maps. *Quart. J. Roy. Meteor. Soc.*, **111,** 877–946.

Houze, R. A., Jr., S. A. Rutledge, M. I. Biggerstaff, and B. F. Smith, 1989: Interpretation of Doppler weather radar displays of midlatitude mesoscale convective systems. *Bull. Amer. Meteor Soc.*, **70,** 608–619.

——, B. F. Smull, and P. Dodge, 1990: Mesoscale organization of springtime storms in Oklahoma. *Mon. Wea. Rev.*, **118,** 613–654.

Jiang, H., and D. J. Raymond, 1995: Simulation of a mature mesoscale convective system using a nonlinear balance model. *J. Atmos. Sci.*, **52,** 161–175.

Johnson, R. H., and P. J. Hamilton, 1988: The relationship of surface pressure features to the precipitation and airflow structure of an intense midlatitude squall line. *Mon. Wea. Rev.*, **116,** 1444–1472.

——, and D. L. Bartels, 1992: Circulations associated with a mature-to-decaying midlatitude mesoscale convective system. Part II: Upper-level features. *Mon. Wea. Rev.*, **120,** 1301–1320.

——, S. Chen, and J. J. Toth, 1989: Circulations associated with a mature-to-decaying midlatitude mesoscale convective sytem. Part I: Surface features—Heat bursts and meso-low development. *Mon. Wea. Rev.*, **117,** 942–959.

Kain, J. S., and J. M. Fritsch, 1990: A one-dimensional entraining/detraining plume model and its application in convective parameterization. *J. Atmos. Sci.*, **47,** 2784–2802.

Kuo, H. L., 1965: On the formation and intensification of tropical cyclones through latent heat release by cumulus convection. *J. Atmos. Sci.*, **22,** 40–63.

——, 1974: Further studies of the parameterization of the influence of cumulus convection on large-scale flow. *J. Atmos. Sci.*, **31,** 1232–1240.

Leary, C.A., and E. M. Rappaport, 1987: The lifecycle and internal structure of a midlatitude mesoscale convective complex. *Mon. Wea. Rev.*, **115,** 1503–1527.

Maddox, R. A., 1980: Mesoscale convective complexes. *Bull. Amer. Meteor. Soc.*, **61,** 1374–1387.

——, 1983: Large scale meteorological conditions associated with midlatitude mesoscale convective complexes. *Mon. Wea. Rev.*, **111,** 1475–1493.

McAnelly, R. L., and W. R. Cotton, 1986: Meso-β scale characteristics of an episode of meso-*a* scale convective complexes. *Mon. Wea. Rev.*, **114,** 1740–1770.

Meitín, J. G., and J. B. Cunning, 1985: The Oklahoma–Kansas Preliminary Regional Exteriment for STORM-Central (OK-PRESTORM), Vol. 1. Daily operations summary. NOAA Tech. Memo. ERL ESG-20, 313 pp. [Available from Department of Commerce, Weather Research Program, Boulder, CO 80303.]

Mellor, G.L., and T. Yamada, 1974: A heiarchy of turbulence closure models for planetary boundary-layers. *J. Atmos. Sci.*, **31,** 1791–1806.

Menard, R. D., and J. M. Fritsch, 1989: A mesoscale convective complex-generated warm core vortex. *Mon. Wea. Rev.*, **117,** 1237–1261.

National Weather Service, 1982: *National Weather Service radar code user's guide*. U.S. Govt. Printing Office. 3 pp.

Olsson, P. Q., and W. R. Cotton, 1997: Balanced and unbalanced circulations in a primitive equation simulation of a midlatitude MCC. Part II: Analysis of balance. *J. Atmos. Sci.*, **54,** 479–497.

Pielke, R. A., and Coauthors, 1992: A comprehensive meteorological modeling system-RAMS. *Meteor. Atmos. Phys.*, **49,** 69–91.

Raymond, D. J., 1992: Nonlinear balance and potential vorticity thinking at large Rossby number. *Quart. J. Roy. Meteor. Soc.*, **118,** 987–1015.

Rutledge, S. A., 1991: Middle latitude and tropical mesoscale convective systems. *Rev. Geophys., Supplement 1: U.S. National Report to International Union of Geodesy and Geophysics 1987–1990*.

Schmidt, J. M., 1992: Numerical and observational investigations of long-lived, MCS-induced, severe surface wind events. The Derecho. Dept. of Atmos. Sci. Paper No. 479, 196 pp. [Available from Department of Atmospheric Science, Colorado State University, Fort Collins, CO 80523-1371.]

——, and W. R. Cotton, 1989: A High Plains squall line associated with severe surface winds. *J. Atmos. Sci.*, **46,** 281–302.

Skamarock, W. C., M. L. Weisman, and J. B. Klemp, 1994: Three-dimensional evolution of simulated long-lived squall lines. *J. Atmos. Sci.*, **51,** 2563–2584.

Smull, B. F., and R. A. Houze, Jr., 1985: A midlatitude squall line with a trailing region of stratiform rain. *Mon. Wea. Rev.*, **113,** 117–133.

——, and ——, 1987a: Dual-Doppler radar analysis of a midlatitude squall line with a trailing region of stratiform rain. *J. Atmos. Sci.*, **44,** 2128–2148.

——, and ——, 1987b: Rear inflow in squall lines with trailing stratiform precipitation. *Mon. Wea. Rev.*, **115,** 2869–2889.

Srivastrava, R. C., T.J. Matejka, and T.J. Lorello, 1986: Doppler radar study of the trailing anvil region associated with a squall line. *J. Atmos. Sci.,* **43,** 356–377.

Stensrud, D. J., and R. A. Maddox, 1988: Opposing mesoscale circulations: A case study. *Wea. Forecasting,* **3,** 189–204.

Tremback, C. J., and R. Kessler, 1985: A surface temperature and moisture parameterization for use in mesoscale numerical models. Preprints, *Seventh Conf. on Numerical Weather Prediction,* Montreal, Quebec, Canada., Amer. Meteor. Soc., 355–358.

Velasco, I., and J.M. Fritsch, 1987: Mesoscale convective complexes in the Americas. *J. Geophys. Res.,* **92,** 9599–9613.

Verlinde, J., and W. R. Cotton, 1990: A mesovortex couplet in the trailing anvil region of a multi-cellular convective complex. *Mon. Wea. Rev.,* **118,** 993–1010.

Walko, R. L., C. J. Tremback, R. A. Pielke, and W. R. Cotton, 1995: An interactive nesting algorithm for stretched grids and variable nesting ratios. *J. Appl. Meteor*., **34,** 994–999.

Weisman, M. L., 1992: The role of convectively generated rear-inflow jets in the evolution of long-lived mesoconvective systems. *J. Atmos. Sci.,* **49,** 1826–1847.

——, 1993: The genesis of severe long-lived bow echoes. *J. Atmos. Sci.,* **50,** 645–670.

——, J. B. Klemp, and R. Rotunno, 1988: Structure and evolution of numerically simulated squall lines. *J. Atmos. Sci.,* **45,** 1990–2013.

Weissbluth, M. J., and W. R. Cotton, 1993: The representation of convection in mesoscale models. Part I: Scheme fabrication and calibration. *J. Atmos. Sci.,* **50,** 3852–3872.

Zhang, D.-L., and J. M. Fritsch, 1987: Numerical simulation of a meso-β scale structure and evolution of the 1977 Johnstown Flood. Part II: Inertially stable warm-core vortex and the mesoscale convective complex. *J. Atmos. Sci.,* **44,** 2593–2612.

——, and ——, 1988: A numerical investigation of a convectively generated, inertially stable, extratropical warm-core mesovortex over land. Part I: Structure and evolution. *Mon. Wea. Rev.,* **116,** 2660–2687.

——, K. Gao, and D. B. Parsons, 1989: Numerical simulation of an intense squall line during 10–11 June 1985 PRE-STORM. Part I: Model verification. *Mon. Wea. Rev.,* **117,** 960–994.

——, J. S. Kain, J. M. Fritsch, and K. Gao, 1994: Comments on ''Parameterization of convective precipitation in mesoscale numerical models: A critical review.'' *Mon. Wea. Rev.,* **122,** 2222–2233.